Plakophilin 2 Couples Actomyosin Remodeling to Desmosomal Plaque Assembly via RhoA

Lisa M. Godsel, Adi D. Dubash, Amanda E. Bass-Zubek, Evangeline V. Amargo, Jodi L. Klessner, Ryan P. Hobbs, Xinyu Chen,* and Kathleen J. Green

Northwestern University Feinberg School of Medicine, Departments of Pathology and Dermatology, and the R. H. Lurie Cancer Center, Chicago, IL 60611

Plakophilin 2 (PKP2), an armadillo family member closely related to p120 catenin (p120ctn), is a constituent of the intercellular adhesive junction, the desmosome. We previously showed that PKP2 loss prevents the incorporation of desmosome precursors enriched in the plaque protein desmoplakin (DP) into newly forming desmosomes, in part by disrupting PKC-dependent regulation of DP assembly competence. On the basis of the observation that DP incorporation into junctions is cytochalasin D–sensitive, here we ask whether PKP2 may also contribute to actin-dependent regulation of desmosome assembly. We demonstrate that PKP2 knockdown impairs cortical actin remodeling after cadherin ligation, without affecting p120ctn expression or localization. Our data suggest that these defects result from the failure of activated RhoA to localize at intercellular interfaces after cell–cell contact and an elevation of cellular RhoA, stress fibers, and other indicators of contractile signaling in squamous cell lines and atrial cardiomyocytes. Consistent with these observations, RhoA activation accelerated DP redistribution to desmosomes during the first hour of junction assembly, whereas sustained RhoA activity compromised desmosome plaque maturation. Together with our previous findings, these data suggest that PKP2 may functionally link RhoA- and PKC-dependent pathways to drive actin reorganization and regulate DP–IF interactions required for normal desmosome assembly.

INTRODUCTION

Adherens junctions and desmosomes are intercellular adhesive junctions that tether the actin and intermediate filament (IF) cytoskeletons, respectively, to the plasma membrane. These junctions cooperate to integrate cell–cell adhesion and cytoskeletal organization and function within tissues. Intercellular adhesion is mediated by transmembrane adhesive receptors that belong to the cadherin family of calcium-dependent adhesion molecules. The cytoplasmic domains of these receptors interact with a complex of proteins to form a junctional plaque, composed of armadillo family members and cytoskeletal adaptors that anchor actin or IF to the membrane (for reviews see Green and Simpson, 2007; Garrod and Chidgey, 2008; Desai et al., 2009).

Evidence suggests that adherens junctions and desmosomes depend on each other for their proper assembly and maintenance. Historically, the majority of data indicates that adherens junctions, which assemble first in response to cell contact, provide structural or signaling cues to guide the formation of desmosomes (O'Keefe et al., 1987; Lewis et al., 1997). More recently it was shown that the loss of desmosomes or desmosome components results in defects in the maturation of adherens junction–based contacts and the associated cortical actin cytoskeleton (Vasioukhin et al., 2001). In turn, desmosomes have been shown to require an intact actin cytoskeleton (Pasdar and Li, 1993). In certain cases, notably in the postnatally remodeled intercalated discs of the heart, adherens junction and desmosome components are intermixed in the same structure, rather than segregating into entirely distinct plasma membrane domains (Goossens et al., 2007; Pieperhoff and Franke, 2008; Bass-Zubek et al., 2009). The molecular mechanisms that couple these two junction types structurally and functionally are poorly understood.

In desmosomes, a member of the plakin family of cytolinkers called desmoplakin (DP), serves as a core constituent of the plaque complex. DP anchors IF to the plasma membrane by its C-terminus and is tethered indirectly to the plasma membrane cadherins by its N-terminus. N-terminal tethering of DP is facilitated by partner proteins in the armadillo family, including plakoglobin and the plakophilins 1–3 (PKPs; Stappenbeck et al., 1993; Kouklis et al., 1994; Meng et al., 1997; Smith and Fuchs, 1998; Choi et al., 2002; Fontao et al., 2003; Jefferson et al., 2004). This DP-dependent link between IF and the plasma membrane is necessary for strong cell–cell adhesion and tissue integrity (Gallicano et al., 1998; Vasioukhin et al., 2001; Huen et al., 2002). Further, mutations in DP and PKPs result in skin fragility and arrhythmogenic right ventricular cardiomyopathy (ARVC), highlighting their important functions in tissue homeostasis (Grossmann et al., 2004; Bolling and Jonkman, 2009). How-

ever, the extent to which defects in the assembly and morphogenesis of desmosomes contributes to disease pathogenesis is not well understood.

Of the desmosomal armadillo proteins associated with the DP N-terminal tethering complex, we know least about specific functions of the PKPs. The PKPs are a subclass of the p120ctn family of armadillo proteins with nine central, fairly well-conserved armadillo repeat domains flanked by less well-conserved amino and carboxy-terminal domains (Bass-Zubek et al., 2009). PKPs are somewhat promiscuous in their partnerships, and through interactions with the desmosomal cadherins, plakoglobin, DP, and IF, they link cadherin tails to the cytoskeleton and also facilitate lateral expansion of the junctional plaque (Bornslaeger et al., 2001; Chen et al., 2002; Bonne et al., 2003; Wahl, 2005; Sobolik-Delmaire et al., 2006; Hatzfeld, 2007; Sobolik-Delmaire et al., 2007). Furthermore, PKPs are involved in junction-independent and signaling functions, as they exhibit both cytoplasmic and nuclear localization and have been shown to associate with nuclear and regulatory proteins (Mertens et al., 2001; Hofmann et al., 2006; Bass-Zubek et al., 2009).

Previously, we showed that cell–cell contact in cultured keratinocytes triggers three phases of desmosomal plaque assembly. Phase I involves the rapid accumulation of DP at contacting borders and is followed by phase II in which nonmembrane bound DP-containing particles enriched in PKP2 form in the cortical region of the cell. These precursors subsequently exhibit slow, directed, anterograde movement to nascent cell–cell contacts in phase III. This DP movement is MT-independent but requires microfilaments and proper regulation of DP's interactions with IF (Godsel et al., 2005). PKP2 is necessary for the normal accumulation of DP in desmosomes of epithelial cells. We recently suggested that this may be due in part to PKP2's function in recruiting protein kinase C alpha (PKCα) to DP, which in turn attenuates DP's interactions with cytoplasmic IF to promote its assembly competence (Bass-Zubek et al., 2008).

DP translocation also requires a correctly organized actin cytoskeleton (Godsel et al., 2005). This cytoskeletal system undergoes dramatic reorganization and remodeling initiated by cell–cell contact, after which thin circumferential actin bundles coalesce to join junctional-associated cortical actin, and previously existing perpendicular actin bundles are incorporated into the cortical actin ring (Zamansky et al., 1991; Vasioukhin et al., 2000; Vaezi et al., 2002; Ivanov et al., 2004, 2005; Shewan et al., 2005; Zhang et al., 2005). In the present study we investigated whether, in addition to regulating DP's interaction with the IF cytoskeleton, PKP2 also participates in actin remodeling to promote desmosome assembly. We show that a pool of PKP2 appears at newly forming cell–cell junctions, in concert with E-cadherin (Ecad) and before DP, during the early stages of actin rearrangement. Loss of PKP2 results in failure of the circumferential actin bundles to coalesce beneath the forming adherens junction. These structural defects in the actin cytoskeleton are accompanied by a failure of RhoA to concentrate at cell–cell interfaces, and an overall elevation of cellular RhoA and downstream indicators of contractile signaling. Consistent with this, activation of RhoA accelerated DP assembly into desmosomes during the first hour of assembly, but its sustained elevation had a negative impact on junctions over time. These data suggest that in addition to the proposed role for RhoA in expansion of cell–cell contacts during adherens junction maturation (Vaezi et al., 2002; Yamada and Nelson, 2007), its proper localization by PKP2 may couple adherens junction assembly to the translocation of desmosome plaque precursors to nascent desmosomes.

MATERIALS AND METHODS

DNA Constructs and Small Interfering RNA

Flag-tagged PKP2 has been described previously (Chen et al., 2002). Full-length human small interfering RNA (siRNA)-resistant PKP2.FLAG (p1376) has been described previously (Bass-Zubek et al., 2008). To generate enhanced green fluorescent protein (EGFP)-tagged PKP2 (p1381) and mCherry-tagged PKP2 (p1383) in LZRS for epithelial cell transduction human PKP2 was amplified from a cDNA library and cloned first into pCMV5a.FLAG (p915). PKP2 was subsequently amplified from p915 and subcloned into pEGFP-C1 to generate p964. Retroviral vectors LZRS-EGFP and LZRS-mCherry were generated by removing the fluorescent tags from pEGFP-C1 and pm-Cherry-C1 and ligating them into LZRS-pBMN (p989). The human PKP2 from p964 was ligated into LZRS-pEGFP to generate p1381 and into LZRS-pm-Cherry to generate p1383. Human actin-pmCherry (p1246), a gift from Shin-ichiro Kojima (Gakushuin University, Tokyo Japan) and Gary Borisy (Marine Biological Laboratory, Woods Hole, MA) was ligated into an LZRS-shuttle vector to generate p1263, followed by ligation into LZRS to generate p1309. The DP.GFP construct and the inducibly expressing cells used in the live cell imaging experiments have been described previously (Godsel et al., 2005). Ecad.red fluorescent protein (RFP) was a gift from W. J. Nelson (Stanford University, Palo Alto, CA) and used to construct LZRS-Ecad-EGFP (p1400) by subcloning the Ecad sequence into pEGFP-N1 followed by ligation of the Ecad-EGFP insert into the LZRS-pBMN retroviral vector. For Ecad-mCherry (p1401) the EGFP tag from p1400 was replaced by the mCherry tag from the pmCherry vector.

Construction of the glutathione S-transferase (GST)-tagged Rhotekin Rho-binding domain (GST-RBD) prokaryotic expression construct was described in Dubash et al. (2007), and this construct, the nucleotide-free GST-RhoA mutant (G17A), and the EGFP-RBD plasmid were the gifts of K. Burridge (University of North Carolina at Chapel Hill). siRNA against human PKP2, against human p120ctn and nontargeting siRNAs were used for knockdown (KD) experiments (Thermo Fisher Scientific, Waltham, MA).

Cell Lines and Transfections

The SCC9 and SCC12f cell lines (gifts of L. Hudson, University of New Mexico; originally isolated by J. Rheinwald, Harvard Medical School, Boston, MA) were maintained in DME/F-12, 10% FBS, and 1% penicillin/streptomycin. The SCC68 cell line was maintained in keratinocyte serum-free media (KSFM) with 0.09 mM Ca^{2+} and supplemented with 1 ml bovine pituitary extract and 0.3 ng/ml epidermal growth factor (EGF; Invitrogen, Carlsbad, CA). Cells were moved to media containing 1.8 mM Ca^{2+} for specified time points before fixation. The HL-1 atrial cardiomyocyte cell line was maintained in Claycomb medium, supplemented with 10% FCS, P/S (100 μg ml^{-1}), epinephrine (0.1 mM) and L-glutamine (2 mM) as previously described (Claycomb et al., 1998). Transient transfections of cDNAs encoding for GFP- or FLAG-tagged proteins were performed on cultures grown on glass coverslips, or on 100- or 35-mm tissue culture dishes (Thermo Fisher Scientific) using Exgen 500 reagent, following the manufacturer's protocol (Fermentas Life Sciences, Glen Burnie, MD). siRNAs were transfected using Dharmafect1 reagent (Thermo Fisher Scientific) following the manufacturer's protocol.

Calcium Switch Treatments

Cells were incubated in low calcium medium (KSFM or DME with 0.09 or 0.05 mM $CaCl_2$, respectively) for 16–24 h and then switched to normal growth media containing >1.8 mM Ca^{2+} to induce cell junction assembly for time periods ranging from 10 min up to 90 min and processed for immunofluorescence or western blotting analyses.

Antibodies and Chemical Reagents

The following rabbit polyclonal antibodies were used: NW6, anti-DP (Angst et al., 1990); 795, anti-Ecad (gift from R. Brackenbury, University of Cincinnati College of Medicine); anti-FLAG (Sigma-Aldrich, St. Louis, MO); phospho-MLC (Cell Signaling Technology, Beverly, MA); total-MLC (Abcam, Cambridge, MA); p-ERM (Cell Signaling Technology); p-MYPT (Millipore, Bedford, MA). The following mouse monoclonal antibodies were used: 12G10, anti-tubulin (provided by J. Frankel and E. M. Nelson from the Developmental Studies Hybridoma Bank under the auspices of the National Institute of Child Health and Human Development and maintained by the University of Iowa, Department of Biological Sciences, Iowa City, IA); clones PP2/62, PP2/86, PP2/150 anti-PKP2 supernatant (Progen Biotechnik, Heidelberg, Germany); anti-p120ctn (BD Transduction Laboratories, Lexington, KY); HECD-1, anti-Ecad (gift from M. Takeichi and O. Abe, Tokyo, Japan; Shimoyama et al., 1989); 6D8, anti-desmoglein 2 (gift from M. Wheelock, K. Johnson, J. Wahl, University of Nebraska Medical Center, Omaha, NE); 26C4, anti-RhoA (Santa Cruz Biotechnology, Santa Cruz, CA); anti-p190RhoGAP antibody (BD Biosciences, San Jose, CA); anti-phosphotyrosine, pY99 (Santa Cruz Biotechnology). The following rabbit monoclonal antibodies were used: anti-p120ctn (Epitomics, Burlingame, CA); p-cofilin (Ser3; Cell Signaling Technology). Photostable, Alexa Fluor–conjugated secondary antibodies were used for indirect immunofluorescence analyses (Invitrogen, Carls-

bad, CA). The following secondary antibodies were used: Alexa Fluor 488 and 568 goat anti-mouse or goat anti-rabbit IgG at 1:300 for immunofluorescence analyses (Invitrogen) and HRP-conjugated goat anti-mouse or goat anti-rabbit IgG at 1:5000 for Western blotting (Kirkegaard Perry Laboratories, Baltimore, MD). Actin was visualized in these analyses using Alexa Fluor 350–, 488–, or 568–conjugated phalloidin at 1:30 (Invitrogen). Blebbistatin (EMD Biosciences, San Diego, CA) was diluted in DMSO to 25 mM and stored as a stock solution and added to cultures at a 1:1000 dilution into culturing medium for a final concentration of 25 μM. Lysophosphatidic acid (LPA; Sigma) was diluted in PBS with 0.1% bovine serum albumin and added to cells at a final concentration of 10 μM.

Preparation of Cell Lysates for Immunoprecipitation and Immunoblot Analysis

Whole cell lysates in Laemmli sample buffer were resolved by 7.5 or 14% SDS-PAGE and immunoblotted as previously described in Angst *et al.* (1990). Immunoreactive proteins were visualized using enhanced chemiluminescence. p190RhoGAP was immunoprecipitated by lysing cells with immunoprecipitation buffer (50 mM Tris, 150 mM NaCl, 10 mM MgCl$_2$, 1% Triton X-100, and protease inhibitor cocktail), and then lysates were incubated with anti-p190RhoGAP antibody (BD Biosciences) at 4°C for 60 min followed by complex collection with protein G-Sepharose, washed, and processed for Western blot analysis. Lysates before antibody incubation were held aside to analyze total p190RhoGAP levels. The complexes were probed with phosphotyrosine antibody (pY99) to look at the active fraction of p190RhoGAP.

Guanine Nucleotide Exchange Factor Activity Pulldowns

Affinity precipitation of exchange factors with the nucleotide-free RhoA mutant (G17A) were performed as described (Garcia-Mata *et al.,* 2006; Dubash *et al.,* 2007). Briefly, cells were lysed in 20 mM HEPES, pH 7.6, 150 mM NaCl, 1% Triton X-100, and 5 mM MgCl$_2$, plus protease inhibitors. Equalized lysates were first precleared with 20 μg of purified GST alone (bound to glutathione-Sepharose beads) for 30 min at 4°C, followed by incubation with 20 μg of purified GST-RhoA(17A) for 60 min at 4°C. Samples were then washed in lysis buffer, processed for SDS-PAGE, and silver-stained using the Pierce SilverSNAP Stain kit II.

Immunofluorescence Analysis and Image Acquisition

Cells were seeded onto collagen-coated glass coverslips for at least 24 h before any siRNA or cDNA transfections were performed. Forty-eight to 72 h after transfection coverslips were washed in PBS and fixed for immunofluorescence. Cells shown in Figure 1, C and D, and Figure 5C were fixed in anhydrous methanol for 2 min at −20°C and air-dried briefly followed by processing with HECD-1, NW6, or 6D8. For immunofluorescence detection of RhoA shown in Figure 8 and Supplemental Figure 3, cells were fixed in ice-cold 10% trichloroacetic acid in water for 15 min followed by a 20-min extraction in ice cold 0.2% Triton X-100 as described in Hayashi *et al.* (1999) and Yonemura *et al.* (2004) before processing for immunofluorescence. RhoA localization detected by this method is thought to represent predominantly active RhoA (Takaishi *et al.,* 1995; Yonemura *et al.,* 2004; Piekny *et al.,* 2005). For studies that included the analysis of the actin cytoskeleton in Figures 1, 2, 4, 5, and 7, as well as Figures 3 and 8E, and Supplemental Figure 4, cells were fixed for 10 min in 4% methanol-free formal saline followed by a 20-min extraction in ice cold 0.2% Triton X-100 in PBS before processing for immunofluorescence.

Introduction of exogenous G-actin into permeabilized cells as shown in Supplemental Figure 1 was performed as described previously (Symons and Mitchison, 1991; Kovacs *et al.,* 2002; Ivanov *et al.,* 2004). Briefly, SCC9 cells on coverslips were subjected to calcium switch, and at specified time points the cells were washed in rinsing buffer (138 mM KCl, 4 mM MgCl$_2$, 20 mM HEPES, pH 7.4) followed by permeabilization for 7 min at room temperature in rinsing buffer containing 0.2 mg/ml saponin and 0.7 mg/ml Alexa Fluor 488–conjugated G-actin. Cells were then fixed for 10 min in 4% methanol-free formal saline and permeabilized with 0.2% Triton X-100 for 15 min on ice.

Cells were processed for indirect immunofluorescence with the following antibodies: 795, anti-p120cat mouse and rabbit monoclonals, NW6, HECD-1, 6D8, PP2/62, PP2/86, PP2/150 supernatant, anti-FLAG, and anti-RhoA. Primary/secondary antibody combinations are routinely tested to rule out nonspecific cross-over. Primary antibody incubations were done for 1 h at 37°C in a humid chamber. In the case of anti-RhoA antibody staining, incubations were performed at 4°C overnight in a humid chamber. Secondary antibody incubations and phalloidin staining were done for 30 min at 37°C. In each case control and treatment populations were manipulated identically throughout the experiment. Coverslips were mounted with polyvinyl alcohol (Sigma-Aldrich).

Fixed cells were visualized with a Leica microscope (model DMR, Melville, NY), an LSM 510 confocal microscope (Carl Zeiss Microimaging, Thornwood, NY), or a Leica DMI 6000B inverted microscope. The DMR microscope was fitted with 40× (PL Fluotar, NA 1.0) and 63× objectives (PL APO, NA 1.32), and images were captured with an Orca 100 CCD camera (model C4742-95; Hamamatsu, Bridgewater, NJ) and Metamorph 6.1 imaging software (Mo-

lecular Devices, Sunnyvale, CA). Images captured with the LSM 510 META microscope (Zeiss) were taken using the 100× objective (PLAN APO CHROMAT, NA 1.4) and Zen software version 5,5,0375. The fluorescent dyes were imaged using the multitrack method. Each laser line was collected into individual photomultiplier channels to eliminate fluor bleedthrough. Images captured with the DMI 6000B were captured with the 100× objective (HCX PL APO, NA 1.4) and an ImagEM electron multiplier CCD camera (Hamamatsu) using Simple PCI software (Hamamatsu). Images were cropped, brightened and contrasted for optimal presentation for using Adobe Photoshop CS4 (Adobe, San Jose, CA), and the images were compiled into figures using Adobe Illustrator CS4 (Adobe).

Time-Lapse Imaging of Fluorescently Tagged Actin and Desmosome Constituents or EGFP-RBD

Cells expressing pairs of the fluorescently tagged junction molecules were seeded onto Lab-Tek chambered coverglass slides (Thermo Fisher Scientific). Singly expressing cells within the population were used as internal controls to ensure that no bleed-through from the other fluorescence channel occurred. Cell monolayers were grown to confluence and wounded with a 26-gauge needle and incubated in imaging medium (HBSS, 20 mm HEPES, 1% FBS, 2 mm L-glutamine, 4.5 g/l glucose, and 1× amino acids; recipe courtesy of G. Kreitzer, Weill Medical College of Cornell University, New York, NY). Cells were incubated at 37°C for 60 min before imaging. Time-lapse recordings shown in Figure 1 were obtained at 1-min intervals. Time-lapse recordings shown in Figure 2 and corresponding Videos 2 and 3 were obtained at 10-s intervals. Time-lapse recordings shown in Figure 9 and corresponding Videos 4 and 5 were obtained at 20-s intervals. Cells in Figures 2 and 9 and corresponding Videos 2–5 were imaged within a 37°C environmental control system chamber using 100 W mercury halide fiber optic illumination. Red and green channels were simultaneously captured with a 100× objective (HCX PL APO, NA 1.4) using a MAG Dual-Cam adaptor fitted with two ORCA-ER AG cameras, for on chip multiplication (Hamamatsu). Images were captured using Simple PCI version 6.0 (Hamamatsu), and images were further processed using ImageJ (http://rsb.info.nih.gov/ij/; National Institutes of Health) for cropping and bleach correction. The time-lapse recordings of SCC12f cells expressing DP.GFP and actin.mCherry in Figure 1 and corresponding Video 1 were obtained at 63× (PL APO, NA 1.3) using mercury illumination with the Application Solution Multidimensional Workstation (ASMDW; Leica). The ASMDW uses a DMIRE2 inverted microscope fitted with a CoolSnap HQ (Roper Scientific, Tucson, AZ) camera, a high-precision scanning stage for simultaneous collection of several fields, and a 63× (HCX PL APO, glycerin, NA 1.3) objective fitted with a piezo element for rapid collection of z-stacks (9; 0.5-μm stacks per time point) in a 37°C climate chamber. All images obtained with the ASMDW were processed and deconvolved using a blind deconvolution synthetic algorithm, and z-stacks from each time point were assembled into multi-image projections using system software. Movies were compiled using Metamorph 7.6 imaging software (Molecular Devices) and QuickTime Pro.

Quantification of Temporal Sequence of Junction Protein Border Localization, Fluorescence Intensity and Immunoblot Densitometry

The appearance of fluorescence at forming cell–cell junctions was measured in time-lapse images of cells expressing pairs of the fluorescently tagged proteins corresponding to data shown in Figure 2 and representative Videos 2 and 3. The data for 39 movies was compiled (12 PKP2/DP pairs, 13 Ecad/DP pairs, and 14 Ecad/PKP2 pairs) and plotted using a whisker graph to lower and upper extremes of border appearance and the lower and upper quartiles of the data sets, as well as median border localization onset within the observed population. The appearance of EGFP-RBD at forming cell–cell junctions was observed upon time-lapse imaging of 20 NTsiRNA control cell pairs and 31 PKP2 siRNA KD cell pairs. Representative movies are shown in Figure 9 and Videos 4 and 5. The fluorescence pixel intensity of forming cell–cell borders shown in Figures 1, 3, and 8 was determined by calculating the average pixel intensity within a region of interest made by tracing along the cell–cell contact using Metamorph 7.6 imaging software (Molecular Devices). Images are representative of at least three experiments. Slides were imaged within 3 d after processing for fluorescence and control, and treatment/knock-down conditions were imaged on the same day utilizing the same instruments and exposure settings. Raw, unsaturated 10- and 12-bit images collected using Metamorph software were used for all quantification. For all quantification analyses, >10 random areas, and in many cases 20–25 random areas, per experimental group were imaged with the same exposure time and camera settings. For border intensity measurements and measurements of actin distance across adjacent cells, 30–150 measurements were recorded for randomly selected cell pairs. Only cell pairs in which both cells were knocked down or expressing a rescue construct were included in the quantitative analysis of actin organization. Graphs were generated using Microsoft Office Excel 2007 (Microsoft, Redmond, WA). Error bars for fluorescence pixel intensity measurements represent SEMs. Statistical analyses were performed using student two-tailed *t* test. Densitometric analyses were
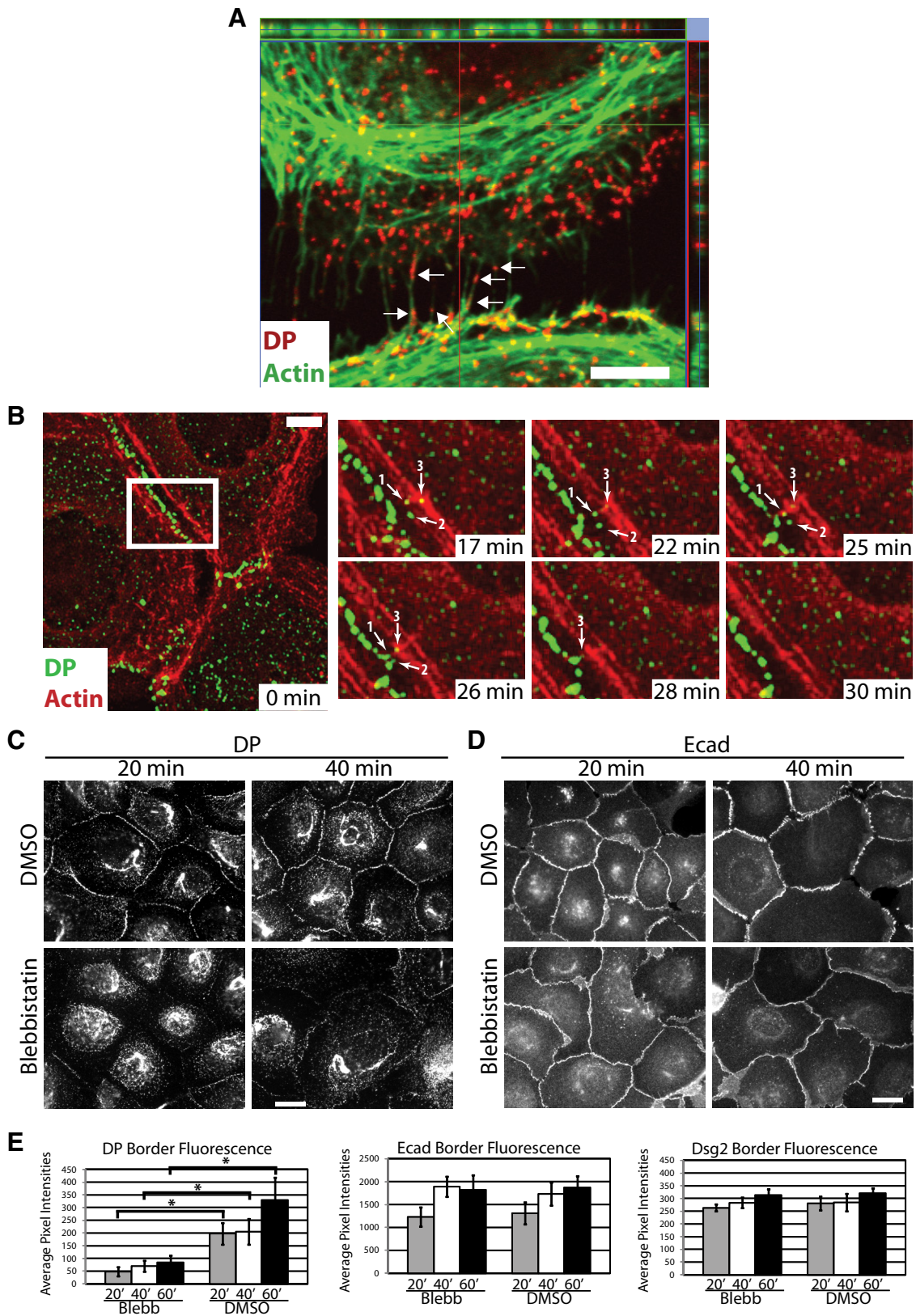
Figure 1. Desmoplakin cytoplasmic particles are found in close proximity to cortical actin and border localization of desmoplakin involves myosin II contractility. (A) SCC9 cells grown overnight in low-calcium medium (0.05 mM) were switched to normal calcium levels for 30 min to induce junction assembly. Cells were fixed with 4% formal saline followed by 0.2% Triton X-100 extraction. Cells were then incubated with primary antibodies against desmoplakin (DP) followed by incubation with Alexa Fluor 568–conjugated secondary antibody and Alexa Fluor 488–labeled phalloidin to visualize actin. DP containing precursor particles are found in close proximity with the actomyosin network (arrows). One XY plane is shown along with the orthogonal planes for the captured Z-stack. Bar, 5 μm. (B) SCC12f cells coexpressing DP.GFP

performed by scanning films using Officejet 5610 scan software (Hewlett-Packard, Palo Alto, CA) and analyzed using ImageJ software (National Institutes of Health). Error bars for densitometric analyses represent SDs.

Purification of Recombinant GST-RBD and RhoA Activity Pulldowns

Construction of the GST-RBD prokaryotic expression construct and purification of the recombinant protein was performed as described in Dubash *et al.*, (2007). Briefly, expression of the fusion proteins in *Escherichia coli* was induced with 100 μM IPTG at room temperature for 12–16 h. The bacteria were pelleted and lysed in 50 mM Tris, pH 7.6, 50 mM NaCl, 5 mM MgCl$_2$, 1% Triton X-100, 1 mM DTT and protease inhibitors (Complete, Roche, Indianapolis, IN). After a brief sonication and preclearing centrifugation step, the lysate was incubated with glutathione-Sepharose 4B beads (GE Healthcare, Waukesha, WI) for 1 h at 4°C. Purified GST-RBD beads were washed in 50 mM Tris, pH 7.6, 50 mM NaCl, 5 mM MgCl$_2$, and 1 mM DTT with protease inhibitors and stored at 4°C. Active RhoA pulldown assays were performed as described in Dubash *et al.* (2007). Briefly, cells were lysed in a buffer containing 50 mM Tris, pH 7.6, 500 mM NaCl, 1% Triton X-100, 0.1% SDS, 0.5% deoxycholate, 10 mM MgCl$_2$, and protease inhibitors. Lysates were clarified by centrifugation at 14,000 rpm for 4–6 min, and total protein concentrations were equalized using the DC Protein Assay Kit (Bio-Rad, Richmond, CA). Samples were then rotated for 30 min at 4°C with 30–60 μg of GST-RBD. The bead pellets were washed in 50 mm Tris, pH 7.6, 150 mM NaCl, 1% Triton X-100, and 10 mM MgCl$_2$ with protease inhibitors and were further processed for SDS-PAGE and Western blotting. G-LISA assays for RhoA activity were performed according to manufacturer's instructions (Cytoskeleton, Denver, CO), and activity was measured using a Synergy 2 plate reader (Biotek, Burlington, VT).

RESULTS

Actomyosin Activity Is Necessary for Desmosome Maturation

Previously we demonstrated that microfilaments are required for the trafficking of discrete DP cytoplasmic precursors to forming desmosomes (Godsel *et al.,* 2005). To more closely analyze the relationship between DP and actin during junction assembly, SCC9 cells were subjected to a calcium switch to initiate junction formation. During the early stages of cell–cell contact formation, endogenous DP-containing particles were observed to be in close proximity with the cortical actomyosin network, and closely aligned with perpendicular actin bundles, as observed in the XY confocal image and included orthogonal planes (Figure 1A). These results are consistent with our previous ultrastructural observations (Green *et al.,* 1987; Godsel *et al.,* 2005) and support a close spatial relationship between desmosome precursors and actin before the process of DP translocation, in addition to their well-characterized association with keratin IF. This close spatial relationship is further illustrated by the anterograde movement of DP particles that are in close proximity with cortical actin during their translocation and incorporation into a maturing cell–cell contact (Figure 1B and Video 1).

The activity of myosin II has been shown to be involved in adherens junction formation (Ivanov *et al.,* 2005; Shewan *et al.,* 2005); however, the potential importance of this motor protein in desmosome formation has not been analyzed. To test whether myosin II–dependent actin contraction is necessary for DP translocation, cells were treated with 25 μM blebbistatin, a myosin II inhibitor (Straight *et al.,* 2003; Kovacs *et al.,* 2004), before and during the formation of cell–cell contacts (Figure 1, C–E). At this low concentration of blebbistatin, both Ecad (Figure 1, D and E) and the desmosomal cadherin, desmoglein 2 (Dsg2; Figure 1E) accumulated at the cell–cell borders with a level of fluorescence intensity similar to that observed for control (DMSO) treated populations. However, DP accumulation was impaired at forming cell–cell borders even after 60 min at normal calcium levels (Figure 1, C and E). That DP accumulation was not completely blocked is likely due to its accumulation through an actomyosin-independent mechanism associated with phase I of desmosome assembly (Godsel *et al.,* 2005). Our previous finding that cytochalasin D impairs desmosomal plaque assembly considered together with these observations, suggest that myosin II–dependent actomyosin contraction participates in DP incorporation into the desmosome.

PKP2 Localizes to Cell–Cell Borders Early upon Junction Formation during Reorganization of the Cortical Actin Cytoskeleton

During the maturation of cell–cell contacts, peripheral, circumferential actin bundles coalesce and incorporate the perpendicular actin bundles observed early in junction assembly into a cortical actin ring, a process requiring the contractile activity of myosin II (Zamansky *et al.,* 1991; Braga *et al.,* 1997; Vasioukhin *et al.,* 2000; Vaezi *et al.,* 2002; Ivanov *et al.,* 2004, 2005; Shewan *et al.,* 2005; Zhang *et al.,* 2005). Because both PKP2 (Bass-Zubek *et al.,* 2008) and actin contractility (Figure 1) were shown to be important for proper junctional assembly of DP, we hypothesized that PKP2 might participate in actin remodeling to help promote the translocation of cytoplasmic DP precursors that occurs during the later phase of desmosome assembly to reinforce the desmosomal plaque (Godsel *et al.,* 2005).

If PKP2 were involved in coupling actin reorganization with the later phase of desmosome assembly, we predicted it would appear at the newly forming borders shortly after initiation of junction assembly. To address this idea, cells were subjected to calcium switch to induce junction formation and then stained with antibodies recognizing Ecad or PKP2, followed by incorporation of fluorescently conjugated phalloidin to observe actin organization (Figure 2A). PKP2 was observed at cell–cell interfaces along with Ecad within 10 min of calcium introduction (Figure 2A, 10 min) and persisted as actin bundles contracted into the mature cortical actin ring (Figure 2A, 60 min).

To determine the pattern of PKP2 accumulation relative to other intercellular junction components with greater temporal resolution, wounded monolayers of epithelial cells expressing pairs of fluorescently tagged PKP2, DP, and Ecad were subjected to time-lapse imaging (Figure 2, B and C; Videos 2 and 3). Time-lapse images were captured at 10-s intervals, and selected images from the time course are shown to illustrate the temporal sequence of junction protein accumulation at sites of cell–cell contact (Figure 2C). The temporal sequence of Ecad, PKP2, and

Figure 1 (cont). and actin.mCherry were wounded and imaged at 1-min intervals after cell–cell contact. DP precursor particles (white arrows, 1–3) move toward contact sites in coordination with the reorganizing junctional actin. The white box in the full field of view (left) is enlarged and shown for six time points illustrating particle movement and actin reorganization. Bar, 10 μm. See also Supplemental Video 1. (C–E) Cells cultured overnight in low-calcium medium were preincubated for 10 min in the presence of 25 μM blebbistatin or DMSO carrier before switching them to normal calcium containing 25 μM blebbistatin for 20-, 40-, and 60-min time points. Cells were fixed with anhydrous methanol and incubated with primary antibodies against DP (C), E-cadherin (Ecad; D), or desmoglein 2 (Dsg2) followed by incubation with Alexa Fluor 488–conjugated secondary antibodies. Bar, 20 μm (E) Average pixel intensities for DP, Ecad, or Dsg2 were quantified along sites of cell–cell contact within the population. Quantitative analyses of immunostained images captured from >10 fields and >30 borders per condition were assessed using Metamorph software; *p < 0.05. The experiments shown are representative of three or more experiments. Although the border localization of Dsg2 and E-cad were unaffected by blebbistatin treatment, DP localization at borders was decreased about four-fold by the inhibition of myosin II.
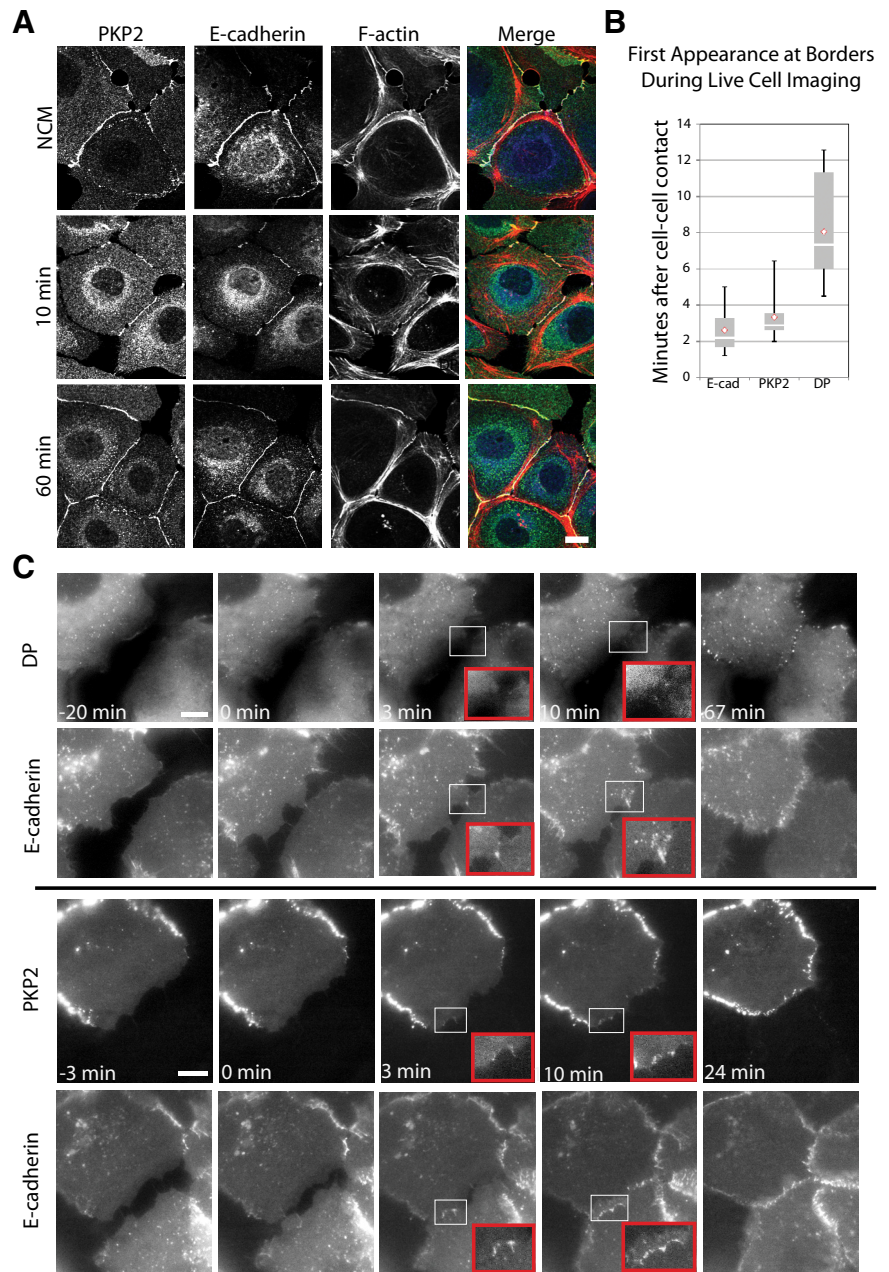
Figure 2. PKP2 is present at cell borders early after cell–cell contact. (A) SCC9s were subjected to calcium switch and then fixed with 4% formal saline followed by 0.2% Triton X-100 extraction at 10 or 60 min and incubated with primary antibodies against PKP2 or E-cadherin (Ecad), followed by incubation with 568 Alexa–conjugated secondary antibodies and phalloidin. Bar, 20 μm. PKP2, Ecad, and actin are all localized at nascent cell–cell contacts within 10 min. (B) SCC9 cells expressing pairs of the junction molecules with GFP- or mCherry-tags were imaged during junction formation. Whisker diagrams demonstrate the temporal sequence of PKP2, Ecad, and DP appearance at nascent cell–cell contacts. On average, Ecad appears at nascent contact sites within 3 min, followed closely by PKP2 at 4 min, whereas DP appears ~10 min after initial cell–cell contact. The experiments shown are a compilation of 39 total experiments. (C) Stills from movies of cells expressing Ecad-mCherry and DP-GFP (top panels) or Ecad-GFP and PKP2-mCherry (bottom panels). Insets, magnification of early cell–cell contacts. Bar, 10 μm. See also Videos 2 and 3. In the Ecad/DP pairing, Ecad appears at sites of cell–cell contact as small puncta within 3 min, whereas DP appears later, within 10 min. In the Ecad/PKP2 pairing Ecad appears at 1½ min after cell contact with PKP2 appearing shortly thereafter at 3 min.

DP border accumulation was analyzed and recorded for 39 movies and illustrated using a whisker plot (Figure 2B). Ecad accumulation at borders occurred on average within 3 min after cell–cell contact, followed closely by PKP2 accumulation at 4 min. DP appeared later, at an average of 8 min after cell–cell contact, consistent with the previously reported first phase of DP accumulation (Godsel *et al.,* 2005). In the pairing shown in Figure 2C, Ecad localized to the cell–cell border within 3 min of the first observed point of cell contact, whereas DP appeared later within 10 min. In the second pairing, Ecad appeared as small puncta at 1½ min after contact with PKP2 appearing at 3 min. Time-lapse analysis of cells coexpressing DP and PKP2 supported this temporal pattern (not shown). The early appearance of PKP2 at sites of nascent junction assembly is consistent with the possibility it may regulate actin dynamics necessary for later stages of desmosome assembly.

PKP2 Is Required for the Proper Reorganization of the Circumferential Actin Ring during Junction Assembly

To more directly address whether PKP2 controls cortical actin remodeling during junction assembly, PKP2 was silenced using an siRNA pool, whereas control cells were transfected with a nontargeting siRNA (NT siRNA). Cell populations were assessed under steady-state conditions or in newly forming borders after a calcium switch. Adherens junction components, including p120ctn, were unchanged in protein level (Figure 3, C and D) and were present in a similar pattern and intensity as control cells at sites of cell–cell contact upon PKP2 KD, although the DP border localization was greatly reduced, as expected (Bass-Zubek *et al.,* 2008; Figure 3, A and B).

On PKP2 silencing, the actin distribution at sites of contact differed from that observed in PKP2-expressing controls (Figure 4, A–F). Junctional actin was observed in a punctate
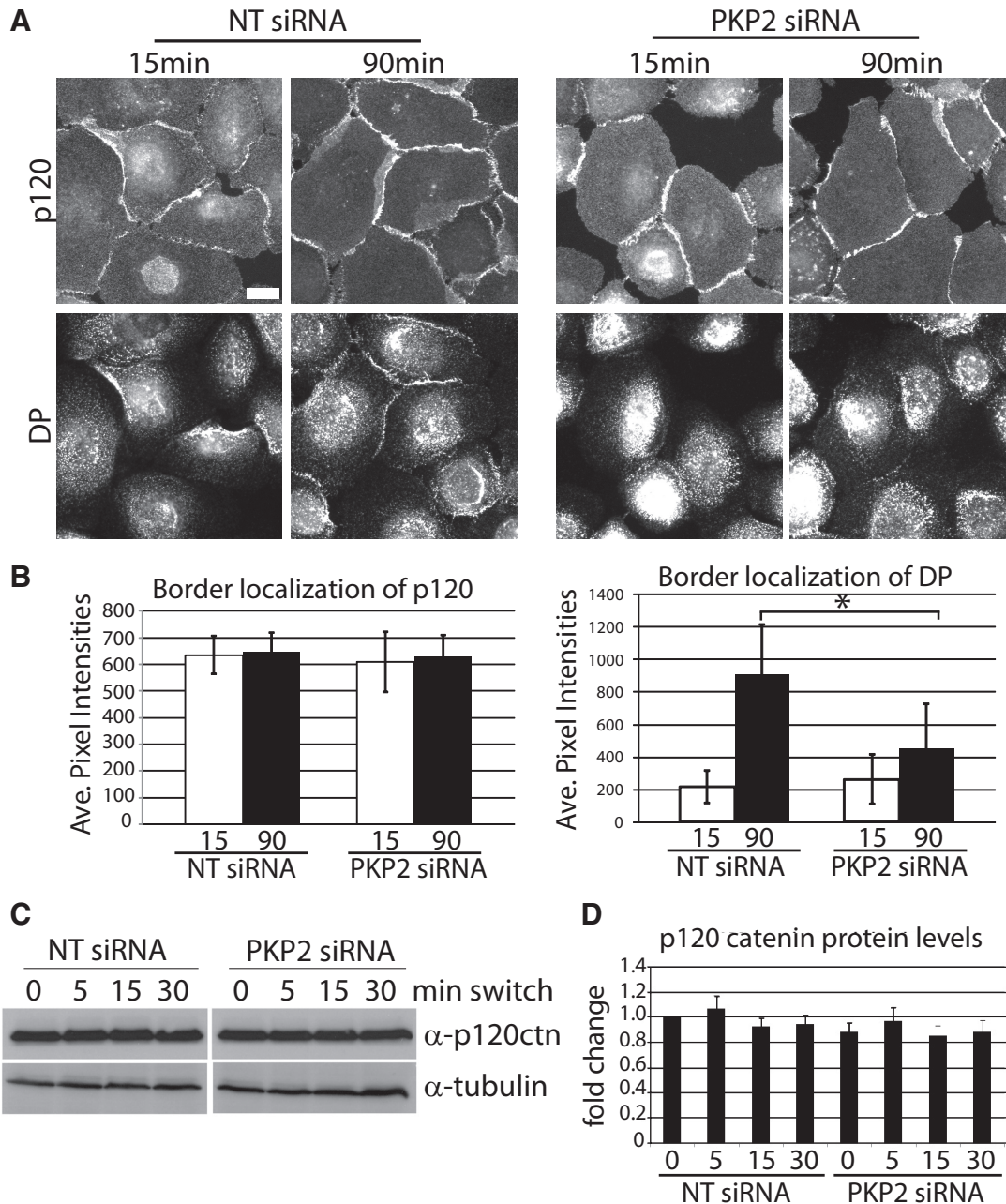
Figure 3. PKP2 KD does not affect the distribution of the adherens junction protein p120ctn. (A) Cells transfected with siRNA against PKP2 or a nontargeting control (NT siRNA) were subjected to a calcium switch for 15 or 90 min and fixed with 4% formal saline followed by 0.2% Triton X-100 extraction. Cells were incubated with primary antibodies against p120ctn or DP followed by incubation with Alexa Fluor 488– and 568–labeled antibodies, respectively. Bar, 20 μm. (B) Average pixel intensities for p120ctn and DP, were quantified along sites of cell–cell contact within the population. Quantitative analyses of immunostained images captured from >10 fields and >40 borders per condition were assessed using Metamorph software; *p < 0.05. The experiments shown are representative of three experiments. Although DP border localization was decreased upon PKP2 KD at 90 min, p120ctn border localization was unaffected. (C) PKP2 KD or the NT siRNA cells were subjected to calcium switch and then harvested at 0-, 5-, 15-, and 30-min time points and analyzed by SDS-PAGE and immunoblotting. p120ctn total levels do not change upon PKP2 KD. (D) Densitometric analysis of the Western blots shown in C.

pattern between the two cells in control cell populations at 60 min after junction formation is induced after a calcium switch. Furthermore, thin cortical actin bundles were found subjacent to the cell membranes (Figure 4A, NTsiRNA). In the absence of PKP2, however, the circumferential actin failed to properly coalesce and concentrate subjacent to the plasma membrane, whereas an increase in actin bundles was observed deeper in the cytoplasm (Figure 4, A–D). This

difference in actin distribution was quantified by measuring the total distance across paired actin bundles in adjacent cells in contact (Figure 4B). Junctional actin formed in both control (NTsiRNA) and PKP2 KD cultures, as G actin was actively incorporated in both cell populations (Supplemental Figure 1B; Zhang *et al.*, 2005). The presence of the perpendicular actin bundles observed in the PKP2 KD cells is not due to cell retraction, or a lack of cell–cell contact, based on
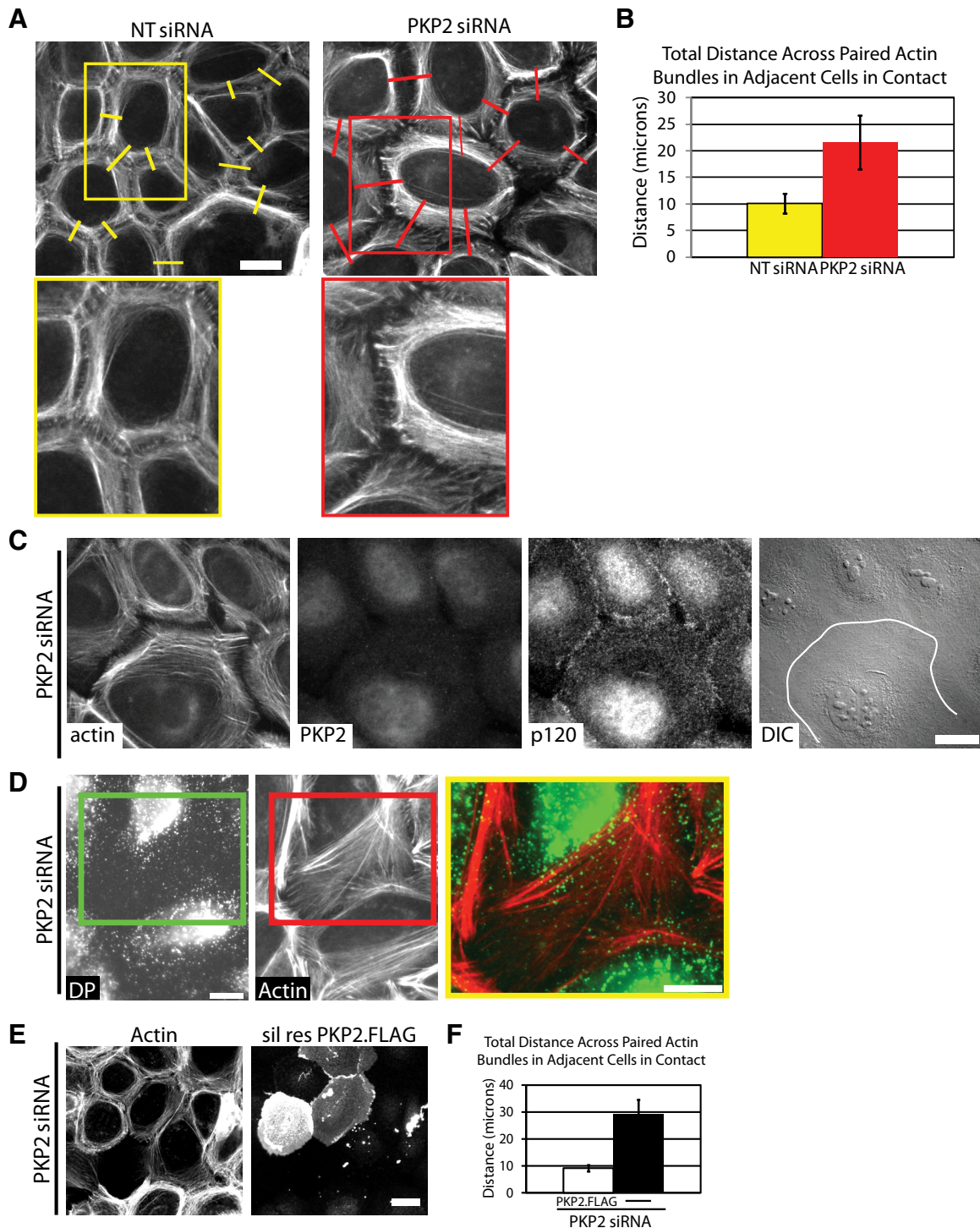
Figure 4. Loss of PKP2 results in changes in cortical actin organization during junction assembly. Cells transfected with siRNA against PKP2 or a nontargeting control (NT-siRNA) were subjected to a calcium switch. Cells were fixed at 60 min with 4% formal saline followed by 0.2% Triton X-100 extraction. (A) Fixed cells were incubated with phalloidin to visualize F-actin. Cortical actin is tightly bundled within 60 min of cell–cell contact as observed in control cells (NT siRNA), whereas PKP2 KD the bundles do not appear as tightly bundled. Bar, 20 μm. (B) The width of paired cortical actin bundles across adjacent cells (includes the space between the bundles and the sum of the two bundles themselves in micrometers); $p < 0.05$. The actin bundles in the PKP2 KD cells cover more distance in the cytoplasm than the cortical actin ring in the control population (NT siRNA). (C) PKP2 KD cells were incubated with primary antibodies against PKP2 and p120ctn, followed by incubation with Alexa Fluor 568– and 488–conjugated secondary antibodies and Alexa Fluor 350 conjugated phalloidin. Bar, 20 μm. Cells are in contact, as indicated by the presence of p120ctn at the maturing cell–cell borders. The region of cell–cell contact is indicated by a white line in the DIC micrograph. (D) PKP2 KD cells were incubated with primary antibodies against DP, followed by incubation with Alexa Fluor 488–conjugated secondary antibodies and Alexa Fluor 568–conjugated phalloidin. Bar, 10 μm. DP containing precursor particles are retained within the loose microfilament bundles in the cell cortex. (E) Cells were transfected with PKP2 siRNA 48 h before being transfected with silencing resistant PKP2-FLAG. Twenty-four hours after the second transfection the cells were subjected to a calcium switch.

the observed maintenance of cell–cell contact by DIC, as well as the presence of p120ctn at cell junctions (Figure 4C). DP-containing particles appeared to be localized in the same area as the widened expanse of actin bundles in the PKP2 KD cells (Figure 4D). The more broad distribution of actin bundles in PKP2 KD cells was unlikely to be due to changes in actin turnover, because cofilin activity was unchanged between the control and PKP2 KD populations (Supplemental Figure 1A). These changes in actin organization were specifically due to the loss of PKP2, because the expression of a silencing-resistant mutant of PKP2 reversed the observed changes in the actin network (Figure 4E). The total distance across paired actin bundles was compared for populations of adjacent PKP2-deficient cells expressing, and not expressing, the silencing resistant PKP2.FLAG construct (Figure 4F).

PKP2 is a member of the p120ctn family of proteins, and p120ctn is known to dramatically affect actin organization when overexpressed in fibroblasts, resulting in generation of multiple filopodia at the cell periphery and stress fiber disruption (Reynolds *et al.*, 1996; Anastasiadis *et al.*, 2000; Noren *et al.*, 2000). However, the reorganization of actin observed upon PKP2 KD was not mimicked by p120 KD (Figure 5, A and B), as p120ctn KD cells exhibited a more condensed cortical actin ring (Figure 5B). Likewise, PKP2 KD affected DP border localization, whereas p120 KD did not affect the localization of DP to nascent cell–cell contacts (Figures 5C and 3, A and B; Bass-Zubek *et al.*, 2008).

Loss of PKP2 Affects the Activity of Myosin Light Chain, a Protein Important for Actin Contractility

To test whether PKP2 regulates the activity of proteins involved in actin organization, such as myosin light chain (MLC), ezrin-radixin-moesin (ERM) proteins and cofilin, we analyzed the activation state of the aforementioned proteins by probing the lysates of control (NT siRNA) and PKP2-silenced (PKP2 siRNA) steady-state cell populations. Loss of PKP2 did not affect the activity of ERM proteins, as assessed by the phosphorylation status of the actin modulators (Figure 6A). Furthermore, neither actin turnover, nor actin deposition appeared to be overtly affected by PKP2 loss, as assessed by cofilin phosphorylation and G actin deposition, respectively (Supplemental Figure 1). However, phosphorylation of MLC, an indicator of contractile signaling, was elevated in the PKP2-silenced population (Figure 6A, pMLC), correlating with the observed increase in broad actin bundles that gave the appearance of stress fibers (Figure 4, A, C, and D; Clark *et al.*, 2007). Correspondingly, we observed an increase in phosphorylation of the phosphatase responsible for inactivating MLC, at a site which results in its inactivation (Figure 6B, pMYPT). Although consistently elevated in PKP2 KD cells compared with controls, MLC phosphorylation was still responsive to the induction of cell–cell

---

Figure 4 (cont). Cells were incubated with antibodies against the FLAG tag followed by incubation with Alexa Fluor 568–conjugated secondary antibodies and Alexa Fluor 488–conjugated phalloidin. Bar, 20 μm. Reintroduction of PKP2-FLAG restores contracted appearance of the cortical actin ring. (F) The total distance (in micrometers) across paired actin bundles in PKP2 KD cells is compared with that in the population of cells expressing the rescue construct. Quantitative analyses of immunostained images captured from >10–15 fields and >40 borders per condition were assessed using Metamorph software; *p < 0.05. The experiments shown are representative of three experiments.
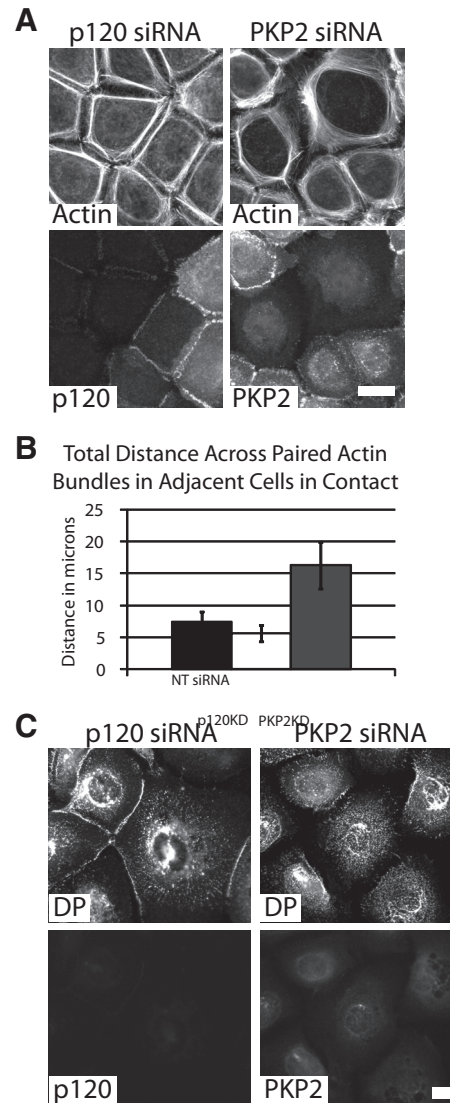

Figure 5. PKP2-mediated changes in actin organization are not shared by p120 cat. (A) Cells were transfected with siRNA against either p120ctn or PKP2 and fixed with 4% formal saline after a 90-min calcium switch. Cells were incubated with antibodies against p120ctn or PKP2 followed by incubation with Alexa Fluor 568–conjugated secondary antibodies and Alexa Fluor 488–conjugated phalloidin. Bar, 20 μm. Although PKP2 KD cells exhibit more widely spaced bundles, p120ctn KD cell actin bundles are more condensed. (B) The width of paired cortical actin bundles of adjacent KD cells (in micrometers). Quantitative analyses of immunostained images captured from >10–15 fields and >80 borders per condition were assessed using Metamorph software; *p < 0.05. (C) Cells transfected with siRNA against either p120ctn or PKP2 were fixed with anhydrous methanol after a 90-min calcium switch. Cells were incubated with primary antibodies against DP and p120ctn or PKP2, followed by incubation with Alexa Fluor 488– and 568–conjugated secondary antibodies, respectively. *p < 0.05. Bar, 20 μm. p120ctn loss does not hinder the localization of DP to cell–cell borders, whereas DP localization is hindered, as expected, upon PKP2 loss (Bass-Zubek *et al.*, 2008). The experiments shown are representative of three experiments.

contact after calcium addition, whereas total MLC protein levels did not change (Figure 6, C and D; Zhang *et al.*, 2005). These data support the idea that PKP2 is involved in the regulation of the actin contractility machinery.
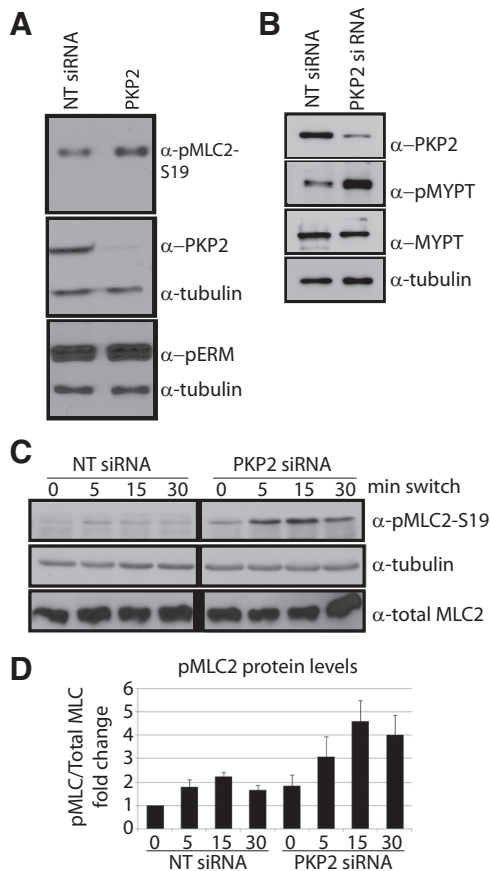
A

NT siRNA   PKP2

α-pMLC2-S19

α—PKP2

α-tubulin

α—pERM

α-tubulin

B

NT siRNA   PKP2 si RNA

α—PKP2

α—pMYPT

α—MYPT

α-tubulin

C

NT siRNA   PKP2 siRNA

0   5   15   30   0   5   15   30   min switch

α-pMLC2-S19

α-tubulin

α-total MLC2

D

pMLC2 protein levels

pMLC/Total MLC fold change

NT siRNA   PKP2 siRNA

Figure 6. The actomyosin contractile machinery is affected by PKP2-deficiency. SCC9 cells were transfected with siRNA against PKP2 or NT siRNA controls and harvested at steady-state conditions (A and B) or harvested after being subjected to calcium switch (C and D). Lysates were subjected to SDS-PAGE and Western blotting and probed for antibodies recognizing the phosphorylated forms of the actin modulating proteins, ERMs and MLC, as well as PKP2, pMYPT, total MLC, and tubulin. Upon PKP2 KD MLC activity increases (A), and the activity of the myosin phosphatase responsible for inactivating MLC decreases (B). (C) MLC phosphorylation (pMLC-S19) increases transiently after calcium switch in both control and PKP2 KD populations. The levels of pMLC are elevated in PKP2 KD at every time point compared with the control, although no change in observed in total MLC levels. (D) Densitometry of the Western blots. The experiments shown are representative of three experiments.

PKP2 Regulates RhoA Activity and Localization during Cell–Cell Contact Formation

The observed alterations in contractile signaling suggest that PKP2 may regulate the activity of the small GTPase, RhoA (Ridley and Hall, 1992; Anastasiadis *et al.,* 2000; Ito *et al.,* 2004; Clark *et al.,* 2007). To begin to address this possibility, we compared actin organization in PKP2-deficient and control cells treated with lysophosphatidic acid (LPA) to activate RhoA (Figure 7, A and B). Similar to PKP2-deficient cells, the control cell population treated with LPA exhibited less concentrated cortical actin staining and an increase in cytoplasmic actin bundles. On the other hand, LPA treatment of the PKP2-silenced cells did not appear to further elevate the already increased number of cortical actin bundles, although their organization was somewhat less regular. To determine if PKP2 KD specifically affects RhoA activity, pulldown assays for GTP-bound RhoA were performed in control or PKP2 KD cells over time after a calcium

switch (Figure 7, C and D). In both control and PKP2 KD populations, RhoA activity was transiently increased within 5 min after addition of calcium; however, RhoA activity was elevated under all conditions in the PKP2 KD cells. Although this increase in RhoA activity is likely due, at least in part, to elevation of total RhoA protein levels in PKP2 KD cells compared with controls, there still is a measurable increase in RhoA activity in the cells when activity is normalized to total levels (Figure 7D, far right graph). This increase in RhoA activity and increase in total levels is also observed in cells consistently maintained in 1.8 mM Ca^{2+} conditions and in multiple cell types, as demonstrated in an HL-1 atrial cardiomyocyte pulldown assay (Figure 7, E and F). Correspondingly, PKP2 overexpression resulted in a decrease in total RhoA activity, as well as a decrease in total protein levels (Figure 7, G–I). These data indicate that RhoA is regulated by PKP2.

p190RhoGAP activity has been linked to the control of p120ctn on RhoA activity (Wildenberg *et al.,* 2006), and a decrease in p190RhoGAP in PKP2-deficient cells could account for this increased RhoA activity we observed. However, p190RhoGAP levels and activity were unchanged in PKP2 KD cells compared with control populations (Supplemental Figure 2A). Next we analyzed the activity profile of RhoA-specific guanine exchange factors (GEFs) to determine if there was a difference in the activity of these proteins, which are responsible for regulating RhoA activity by affecting GDP/GTP exchange. Utilizing a nucleotide-free mutant of RhoA that binds to active GEFs, we did not observe any major change in the GEF activation profile in the PKP2 KD cells compared with control populations (Supplemental Figure 2B). This indicates that PKP2 may not affect Rho activity through regulation of GEFs.

A global increase in RhoA and downstream activation of pMLC upon PKP2 KD initially seemed surprising in light of the failure of cortical actin to undergo myosin-dependent rearrangements after initiation of junction assembly (Clark *et al.,* 2007). We hypothesized that PKP2 may be required for properly localizing RhoA activity to sites of junction assembly. Indeed, although RhoA was concentrated at cell–cell interfaces within 30–45 min of calcium in control cells, it did not accumulate at sites of nascent junction assembly in PKP2-silenced cells (Figure 8, A–C, and Supplemental Figure 3; Takaishi *et al.,* 1995; Yonemura *et al.,* 2004). The localization of RhoA to sites of cell–cell contact was rescued by re-expression of the silencing resistant PKP2-FLAG (Figure 8D). These population studies uncover an accumulation of RhoA at the cell membrane, where RhoA is thought to be active (Piekny *et al.,* 2005). The localization of RhoA by PKP2 could be important for the maturation of the desmosome. Correspondingly, the activation of RhoA by LPA treatment accelerated the redistribution of DP to sites of cell–cell contact during the first hour of assembly (Figure 8E), whereas inhibition of the RhoA downstream effector Rho kinases (ROCK I, II) with Y27632 inhibited DP border accumulation during this time frame (Supplemental Figure 4).

The RhoA staining studies suggest that active RhoA accumulates at the sites of nascent contact. To more accurately determine the temporal localization of active RhoA at nascent cell–cell contact sites, we utilized the Rhotekin Rho-binding domain (RBD) fused to EGFP. By associating with endogenous, active Rho, EGFP-RBD can be used as a marker for active Rho localization and as such accumulates at sites of RhoA activity (Ren *et al.,* 1999; Benink and Bement, 2005; Piekny *et al.,* 2005; Bement *et al.,* 2006). Live cell imaging of control cells expressing the EGFP-RBD construct demonstrated that active Rho is present in lamellar ruffles of both control and PKP2 KD cells (Figure 9B; Video 5; Pertz *et al.,* 2006). However, although EGFP-RBD was observed to ac-
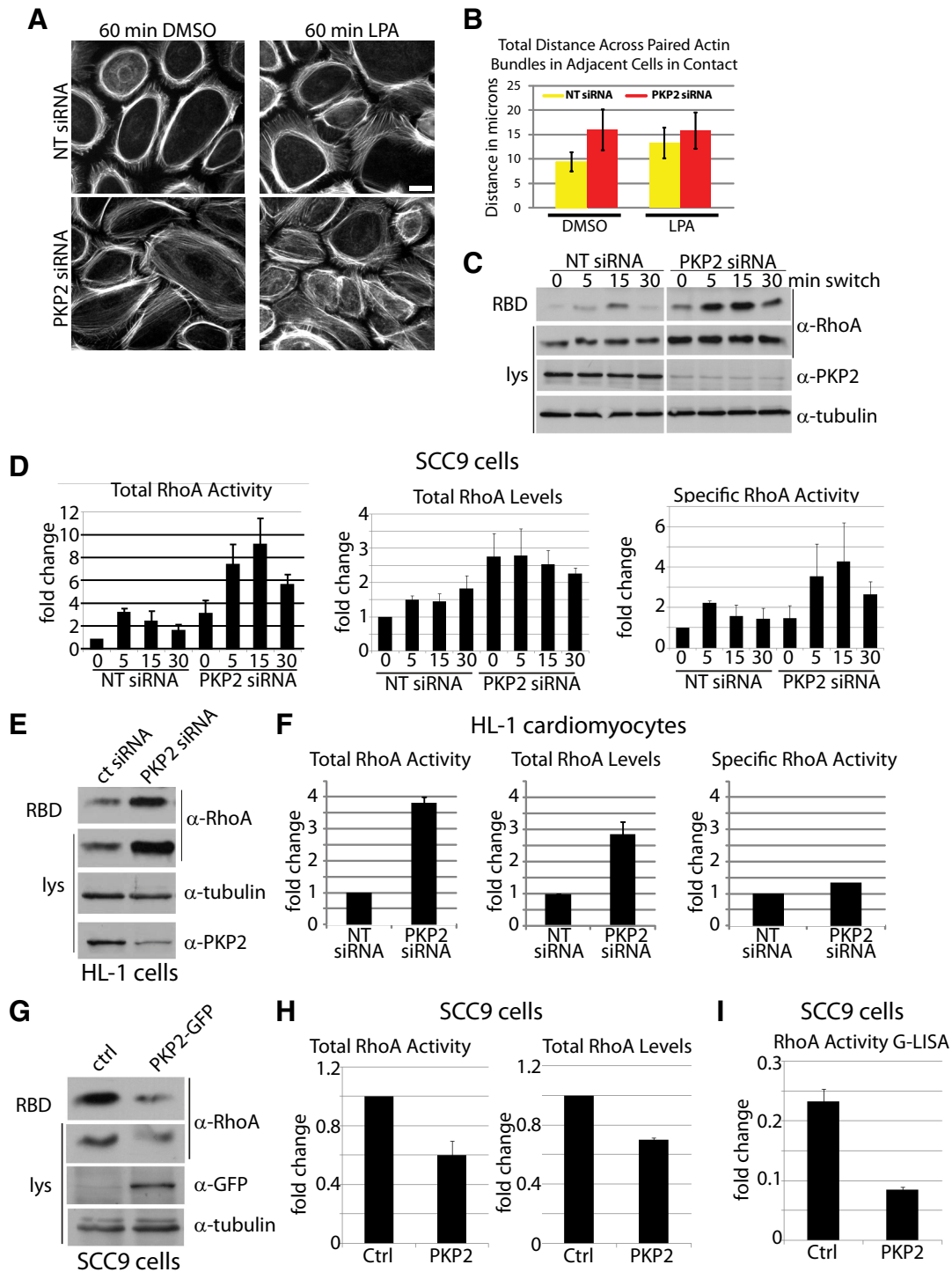
Figure 7. PKP2 KD results in increased RhoA activity. (A) SCC9 cells transfected with siRNA against PKP2 or NT siRNA controls were subjected to a calcium switch assay for 60 min in the presence or absence of the RhoA activator LPA at 10 μM followed by fixation with 4% formal saline and extracted with 0.2% Triton X-100, followed by incubation with Alexa Fluor 488–conjugated phalloidin. Bar, 20 μm. Cortical actin arrangement in LPA-treated NT siRNA cells mimics that observed in the PKP2 KD cells. LPA treatment of PKP2 KD cells resulted in a modest increase in stress fibers beyond the amount observed upon PKP2 KD alone. (B) The width of paired cortical actin bundles across adjacent cells (in micrometers) illustrates that upon LPA treatment the NT siRNA control and PKP2 KD populations are virtually indistinguishable. (C) Cells transfected with siRNA against PKP2 or NT siRNA controls were subjected to a calcium switch assay and harvested at various time points (0–30 min). GST-RBD pulldowns were performed to precipitate GTP-bound RhoA from each lysate. RhoA activity transiently increases in response to calcium in both control and PKP2 KD conditions, although the PKP2 KD cells have an increased in total RhoA levels and an increased level of RhoA activity at all time points examined, which is quantified by densitometry in D and is an average of three independent experiments. (E) HL-1 atrial cardiomyocyte cultures were transfected with siRNA against PKP2 or NT siRNA controls and collected in steady-state conditions for GST-RBD pulldown analysis. RhoA total levels and activity are both increased upon PKP2 KD, which is quantified by densitometry in F. (G) Overexpression of PKP2-GFP in cells decreases the activity of RhoA. GST-RBD
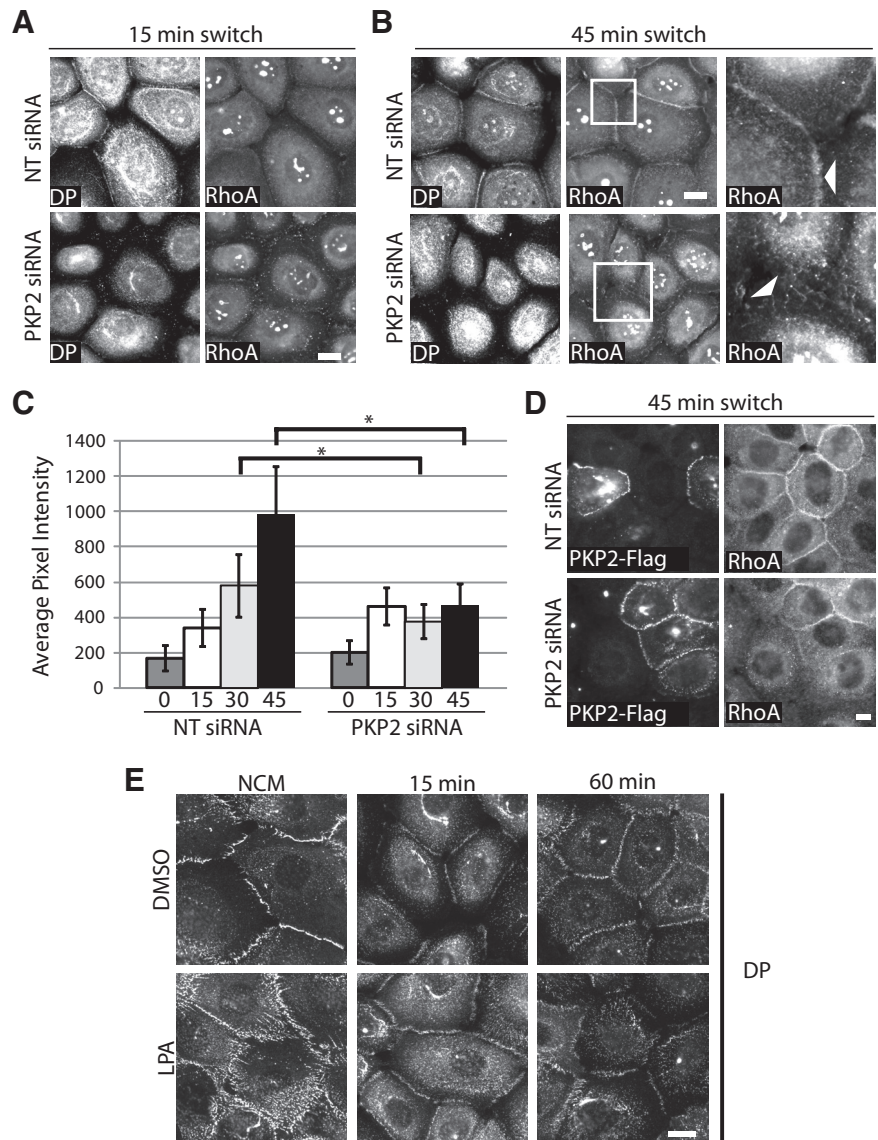
Figure 8. RhoA is mislocalized upon PKP2 loss. Cells transfected with siRNA against PKP2 or NT siRNA controls were subjected to a calcium switch assay (0–45 min) and fixed in 10% TCA followed by 0.2% Triton X-100. Cells were incubated with primary antibodies against DP and RhoA, followed by incubation with Alexa Fluor 568– and 488–conjugated secondary antibodies, respectively. (A and B) Within 45 min after calcium addition RhoA is localized to regions of nascent cell–cell contact in the control population (NT siRNA), whereas it is absent from sites of contact in the PKP2 KD cells. Bar, 20 μm. (C) The fluorescence intensity of RhoA at cell–cell borders was quantified and compared for the NT siRNA control and PKP2 KD populations; *p < 0.05. Quantitative analyses of immunostained images captured from >10–15 fields and >10 borders per condition were assessed using Metamorph software; *p < 0.05. (D) This ability of RhoA to localize to sites of cell–cell contact was rescued by introduction of a silencing resistant PKP2-FLAG construct. Bar, 20 μm. (E) Cells were subjected to a calcium switch (15 and 60 min) or cultured in normal calcium conditions (NCM) in the presence of 10 μM LPA or DMSO vehicle. Cells were fixed with 4% fomal saline and extracted with 0.2% Triton X-100 followed by incubation with primary antibodies against DP and Alexa Fluor–conjugated secondary antibody. Bar, 20 μm. Activation of RhoA via LPA treatment increases the early accumulation of DP at cell–cell contact sites, whereas sustained activity somewhat diminishes DP border accumulation relative to control at 60 min. The experiments shown in the figure are representative of three experiments.

cumulate at nascent cell–cell borders in the control cell population, it failed to do so in PKP2-deficient cells, even though Ecad was present at sites of cell–cell contact (Figure 9A and Videos 4 and 5). This accumulation of active Rho in the control cells was observed on average within 30 min of initial cell–cell contact, corresponding well with RhoA staining of fixed cell populations (Figure 8, A–C). Collectively, these results indicate that PKP2 is required for recruiting active RhoA to sites of actin reorganization before the late phase of DP incorporation into nascent desmosomes. The persistently elevated RhoA activity and its mislocalization from cell–cell borders in PKP2-deficient cells likely contribute to the observed inhibition of cortical actin remodeling and accompanying overall increase in contractile signaling

and stress fibers, resulting in defects in cell–cell junction formation (Ridley and Hall, 1992; Clark et al., 2007).

DISCUSSION

Cell contact triggers a cascade of events in cultured epithelial cells that leads to the formation of adherens junctions, followed closely by the appearance of desmosomes. In response to cell contact, classic cadherin ligation triggers Rho GTPase-induced remodeling of the actin cytoskeleton into parallel cortical actin bundles to aid in formation of a mature junction (Yonemura et al., 1995; Noren et al., 2000; Perez-Moreno and Fuchs, 2006; Pokutta et al., 2008). In keratinocytes, the maturation of desmosomal plaques that occurs by the translocation of newly assembled cytoplasmic desmosomal plaque precursors is a cytochalasin D–sensitive process that is coordinated temporally with adherens junction–driven actin remodeling (Green et al., 1987; Godsel et al., 2005; Figures 2 and 4). Our data presented here suggest that PKP2 contributes to coupling adherens junction maturation with assembly of the desmosomal plaque through its interference with this actin remodeling process.

Figure 7 (cont). pulldowns were performed on cells expressing PKP2-GFP by viral transduction. PKP2-GFP–expressing cells show a decrease in RhoA activity compared with control cells, which is quantified in H. (I) The results in G and H, which were obtained using traditional GST-RBD pulldowns, were confirmed using a G-LISA assay.
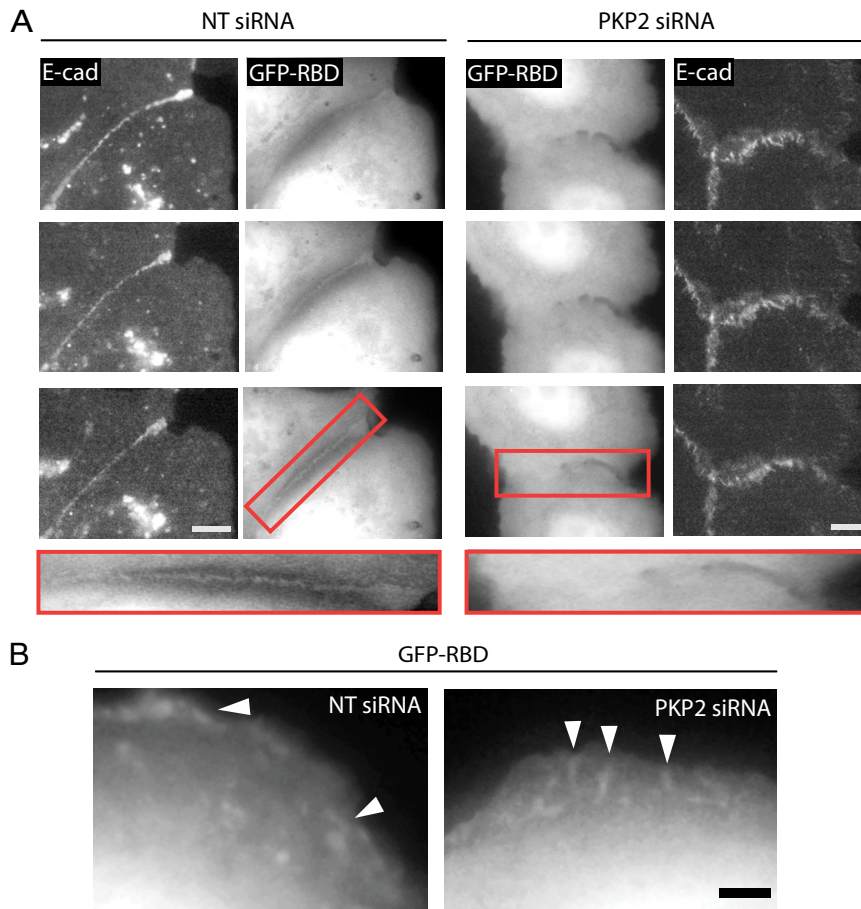
Figure 9. Localization of Rho activity to sites of nascent cell–cell contact requires PKP2 expression. (A) Cells retrovirally transduced to express E-cadherin (E-cad).mCherry were transfected with siRNA against PKP2 or NT siRNA controls followed by a separate EGFP-RBD transfection 24 h before time-lapse imaging. Cells were subjected to a calcium switch assay followed by single plane, live cell imaging at 20-s intervals. EGFP-RBD, which binds to active, endogenous Rho accumulated at sites of cell–cell contact in the control cells, but was not observed to accumulate at the contact site of PKP2 KD cells, although E-cad does. The red boxed area is magnified to show region of cell–cell contact in control (NT siRNA) and PKP2 KD cells. See Videos 4 and 5. Bar, 10 μm. (B) Although active Rho did not accumulate at sites of cell–cell contact in PKP2 KD cells, it was observed in the lamellar ruffles of both control and PKP2 KD cells. See Video 5. Bar, 5 μm. Twenty NT siRNA control cell pairs and 31 PKP2 KD cell pairs were imaged over the course of several weeks for analysis of active Rho accumulation.

Here we show that PKP2 deficiency results an overall increase in RhoA activity and accompanying indicators of contractile signaling (Yonemura *et al.,* 1995; Perez-Moreno and Fuchs, 2006; Pokutta *et al.,* 2008), whereas active RhoA fails to accumulate at cell borders. These alterations in RhoA are accompanied by aberrant cortical actin bundling, and an increase in stress fiber formation. The fact that DP accumulation in junctions is a cytochalasin D– (Godsel *et al.,* 2005) and blebbistatin-sensitive process, coupled with the observation that LPA accelerates DP accumulation during the first hour of junction assembly, is consistent with a model where by PKP2-dependent localization of active RhoA in response to cell contact regulates actin remodeling important for the later stages of desmosomal plaque assembly. Although our data suggest that some DP-rich desmosome precursors maintain a close association with actin as they make their final entry into junctions (Figure 1B, particles 1 and 3), others may enter more indirectly through actomyosin-dependent pulling of IF with associated DP particles into sites of junction assembly.

We propose that PKP2 functionally links the actin- and previously described IF-dependent arms of the DP assembly pathway (Figure 10, model), by 1) acting as a scaffold that brings PKCα in the vicinity of DP to properly modulate its interaction with IF (Bass-Zubek *et al.,* 2009) and 2) to localize RhoA signaling machinery to sites of nascent junction assembly at cell–cell contact sites. RhoA has been reported as being among the many signaling pathways PKC regulates (Holinstat *et al.,* 2003). The fact that PKP2 has an impact on both RhoA and PKC raised the possibility that they are in the same pathway. However, in SCC9 cells RhoA activity

was not affected either by silencing or elevating PKCα activity, nor did these manipulations rescue the changes in
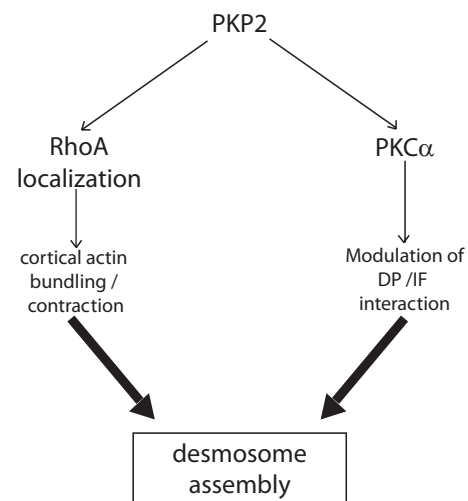

Figure 10. A schematic representation depicting proposed PKP2-dependent pathways important for desmosomal plaque assembly. The data are consistent with a model in which PKP2 orchestrates DP incorporation into desmosomes through two pathways: 1) by acting as a scaffold that recruits PKCα to DP to modulate its interaction with intermediate filaments (IF; Godsel *et al.,* 2005; Bass-Zubek *et al.,* 2008), and 2) by localizing RhoA at sites of nascent junction assembly and regulating cortical actin remodeling necessary for DP accumulation and junction maturation.

actin organization observed upon PKP2 KD (not shown). These results suggest that PKP2 regulates multiple pathways important for cell–cell junction formation and stability, in part by proper localization of these signaling mediators (Figure 10).

PKP2 may also provide a structural link between junctional components and both the actin- and the IF cytoskeletons to properly coordinate their activities during junction assembly. Previous work showed that PKP1 colocalizes with actin (Hatzfeld *et al.*, 2000), and we have observed that full-length PKP2 accumulates on actin stress fibers when expressed in REF52 fibroblasts (not shown). In addition, PKP2 associates with known actin-binding proteins such as α-T-catenin (Goossens *et al.*, 2007) and indirectly associates with Ecad in SCC cells (Chen *et al.*, 2002). PKP2 would thus be spatially and temporally poised to couple Ecad engagement with the contractile signaling machinery to initiate the process of actin remodeling necessary for both adherens junction maturation and desmosomal plaque assembly.

The related armadillo protein p120ctn has also been demonstrated to inhibit RhoA activity (Anastasiadis *et al.*, 2000; Anastasiadis and Reynolds, 2001; Hatzfeld, 2007). Inhibition of RhoA through p190RhoGAP via cadherin-associated p120ctn may ensure that its activity is kept in check at cell–cell junctions during later stages of maturation and at steady state (Wildenberg *et al.*, 2006). We considered the possibility that the observed alterations in RhoA activity observed here might be through alterations in p120ctn protein levels in PKP2-deficient cells. However, p120ctn levels did not change, nor was p120ctn distribution affected in these cells (Figure 3). Furthermore, the actin organization in PKP2-deficient cells differs significantly from that in p120ctn-deficient SCC cells (Figure 5). Finally, PKP2 silencing had no effect on p190RhoGAP activity, PKP2 did not coprecipitate with p190RhoGAP or affect the profile of active GEFs (not shown and Supplemental Figure 2). These data suggest that although both PKP2 and p120ctn have the ability to inhibit RhoA, they do so through different mechanisms and in addition, that other functions of these molecules convert their final activities into phenotypically different signatures.

Another desmosome associated molecule, kazrin, was previously shown to induce similar cell shape changes when overexpressed. Kazrin was identified as a partner of periplakin, a widely expressed plakin family–interacting protein, nonobligate desmosome component, and cornified envelope protein constituent. Although kazrin's cell shape-changing properties were associated with decreased RhoA activity, kazrin-deficient keratinocytes exhibited decreased differentiation markers but no total change in Rho activity (Sevilla *et al.*, 2008).

The regulation of desmosome precursor recruitment via multiple mechanisms provides a way of fine-tuning adhesive strengthening as cell sheets reorganize. Alterations in RhoA and/or PKC signaling may act as rheostats to attenuate the recruitment of DP-containing reinforcements during dynamic remodeling. This attenuation may insure that strengthening does not occur too rapidly while the leading edges of epithelial sheets begin to seal. Loss of PKPs has also been associated with diseases of the skin and heart. In particular, a majority of cases of the disease arrhythmogenic right ventricular cardiomyopathy have been attributed to mutations in PKP2, many of which lead to haploinsufficiency. The observed alterations in both PKC and Rho-dependent cytoskeletal regulation in PKP2-deficient cells raise the possibility that one or both pathways may contribute to disease pathophysiology previously attributed to mechanical impairment of intercellular junctions.

REFERENCES

Anastasiadis, P. Z., Moon, S. Y., Thoreson, M. A., Mariner, D. J., Crawford, H. C., Zheng, Y., and Reynolds, A. B. (2000). Inhibition of RhoA by p120 catenin. Nat. Cell Biol. *2*, 637–644.

Anastasiadis, P. Z., and Reynolds, A. B. (2001). Regulation of Rho GTPases by p120-catenin. Curr. Opin. Cell Biol. *13*, 604–610.

Angst, B. D., Nilles, L. A., and Green, K. J. (1990). Desmoplakin II expression is not restricted to stratified epithelia. J. Cell Sci. *97*(Pt 2), 247–257.

Bass-Zubek, A. E., Godsel, L. M., Delmar, M., and Green, K. J. (2009). Plakophilins: multifunctional scaffolds for adhesion and signaling. Curr. Opin. Cell Biol. *21*, 708–716.

Bass-Zubek, A. E., Hobbs, R. P., Amargo, E. V., Garcia, N. J., Hsieh, S. N., Chen, X., Wahl, J. K., 3rd, Denning, M. F., and Green, K. J. (2008). Plakophilin2, a critical scaffold for PKC alpha that regulates intercellular junction assembly. J. Cell Biol. *181*, 605–613.

Bement, W. M., Miller, A. L., and von Dassow, G. (2006). Rho GTPase activity zones and transient contractile arrays. BioEssays *28*, 983–993.

Benink, H. A., and Bement, W. M. (2005). Concentric zones of active RhoA and Cdc42 around single cell wounds. J. Cell Biol. *168*, 429–439.

Bolling, M. C., and Jonkman, M. F. (2009). Skin and heart: une liaison dangereuse. Exp. Dermatol. *18*, 658–668.

Bonne, S., Gilbert, B., Hatzfeld, M., Chen, X., Green, K. J., and Van Roy, F. (2003). Defining desmosomal plakophilin-3 interactions. J. Cell Biol. *161*, 403–416.

Bornslaeger, E. A., Godsel, L. M., Corcoran, C. M., Park, J. K., Hatzfeld, M., Kowalczyk, A. P., and Green, K. J. (2001). Plakophilin 1 interferes with plakoglobin binding to desmoplakin, yet together with plakoglobin promotes clustering of desmosomal plaque complexes at cell-cell borders. J. Cell Sci. *114*, 727–738.

Braga, V. M., Machesky, L. M., Hall, A., and Hotchin, N. A. (1997). The small GTPases Rho and Rac are required for the establishment of cadherin-dependent cell-cell contacts. J. Cell Biol. *137*, 1421–1431.

Chen, X., Bonne, S., Hatzfeld, M., van Roy, F., and Green, K. J. (2002). Protein binding and functional characterization of plakophilin 2. Evidence for its diverse roles in desmosomes and beta-catenin signaling. J. Biol. Chem. *277*, 10512–10522.

Choi, H. J., Park-Snyder, S., Pascoe, L. T., Green, K. J., and Weis, W. I. (2002). Structures of two intermediate filament-binding fragments of desmoplakin reveal a unique repeat motif structure. Nat. Struct. Biol. *9*, 612–620.

Clark, K., Langeslag, M., Figdor, C. G., and van Leeuwen, F. N. (2007). Myosin II and mechanotransduction: a balancing act. Trends Cell Biol. *17*, 178–186.

Claycomb, W. C., Lanson, N. A., Jr., Stallworth, B. S., Egeland, D. B., Delcarpio, J. B., Bahinski, A., and Izzo, N. J., Jr. (1998). HL-1 cells: a cardiac muscle cell line that contracts and retains phenotypic characteristics of the adult cardiomyocyte. Proc. Natl. Acad. Sci. USA *95*, 2979–2984.

Desai, B. V., Harmon, R. M., and Green, K. J. (2009). Desmosomes at a glance. J. Cell Sci. *122*, 4401–4407.

Dubash, A. D., Wennerberg, K., Garcia-Mata, R., Menold, M. M., Arthur, W. T., and Burridge, K. (2007). A novel role for Lsc/p115 RhoGEF and LARG in regulating RhoA activity downstream of adhesion to fibronectin. J. Cell Sci. *120*, 3989–3998.

Fontao, L., Favre, B., Riou, S., Geerts, D., Jaunin, F., Saurat, J.-H., Green, K. J., Sonnenberg, A., and Borradori, L. (2003). Interaction of the bullous pemphigoid antigen 1 (BP230) and desmoplakin with intermediate filaments is mediated by distinct sequences within their COOH terminus. Mol. Biol. Cell *14*, 1978–1992.

Gallicano, G. I., Kouklis, P., Bauer, C., Yin, M., Vasioukhin, V., Degenstein, L., and Fuchs, E. (1998). Desmoplakin is required early in development for assembly of desmosomes and cytoskeletal linkage. J. Cell Biol. *143*, 2009–2022.

Garcia-Mata, R., Wennerberg, K., Arthur, W. T., Noren, N. K., Ellerbroek, S. M., and Burridge, K. (2006). Analysis of activated GAPs and GEFs in cell lysates. Methods Enzymol. *406*, 425–437.

Garrod, D., and Chidgey, M. (2008). Desmosome structure, composition and function. Biochim. Biophys. Acta *1778*, 572–587.

Godsel, L. M., *et al.* (2005). Desmoplakin assembly dynamics in four dimensions: multiple phases differentially regulated by intermediate filaments and actin. J. Cell Biol. *171*, 1045–1059.

Goossens, S., Janssens, B., Bonne, S., De Rycke, R., Braet, F., van Hengel, J., and van Roy, F. (2007). A unique and specific interaction between alphaT-catenin and plakophilin-2 in the area composita, the mixed-type junctional structure of cardiac intercalated discs. J. Cell Sci. *120*, 2126–2136.

Green, K. J., Geiger, B., Jones, J.C.R., Talian, J. C., and Goldman, R. D. (1987). The relationship between intermediate filaments and microfilaments prior to and during the formation of desmosomes and adherens-type junctions in mouse epidermal keratinocytes. J. Cell Biol. *104*, 1389–1402.

Green, K. J., and Simpson, C. L. (2007). Desmosomes: new perspectives on a classic. J. Invest. Dermatol. *127*, 2499–2515.

Grossmann, K. S., Grund, C., Huelsken, J., Behrend, M., Erdmann, B., Franke, W. W., and Birchmeier, W. (2004). Requirement of plakophilin 2 for heart morphogenesis and cardiac junction formation. J. Cell Biol. *167*, 149–160.

Hatzfeld, M. (2007). Plakophilins: multifunctional proteins or just regulators of desmosomal adhesion? Biochim. Biophys. Acta *1773*, 69–77.

Hatzfeld, M., Haffner, C., Schulze, K., and Vinzens, U. (2000). The function of plakophilin 1 in desmosome assembly and actin filament organization. J. Cell Biol. *149*, 209–222.

Hayashi, K., Yonemura, S., Matsui, T., and Tsukita, S. (1999). Immunofluorescence detection of ezrin/radixin/moesin (ERM) proteins with their carboxyl-terminal threonine phosphorylated in cultured cells and tissues. J. Cell Sci. *112*(Pt 8), 1149–1158.

Hofmann, I., Casella, M., Schnolzer, M., Schlechter, T., Spring, H., and Franke, W. W. (2006). Identification of the junctional plaque protein plakophilin 3 in cytoplasmic particles containing RNA-binding proteins and the recruitment of plakophilins 1 and 3 to stress granules. Mol. Biol. Cell *17*, 1388–1398.

Holinstat, M., Mehta, D., Kozasa, T., Minshall, R. D., and Malik, A. B. (2003). Protein kinase Calpha-induced p115RhoGEF phosphorylation signals endothelial cytoskeletal rearrangement. J. Biol. Chem. *278*, 28793–28798.

Huen, A. C., *et al.* (2002). Intermediate filament-membrane attachments function synergistically with actin-dependent contacts to regulate intercellular adhesive strength. J. Cell Biol. *159*, 1005–1017.

Ito, M., Nakano, T., Erdodi, F., and Hartshorne, D. J. (2004). Myosin phosphatase: structure, regulation and function. Mol. Cell Biochem. *259*, 197–209.

Ivanov, A. I., Hunt, D., Utech, M., Nusrat, A., and Parkos, C. A. (2005). Differential roles for actin polymerization and a myosin II motor in assembly of the epithelial apical junctional complex. Mol. Biol. Cell *16*, 2636–2650.

Ivanov, A. I., McCall, I. C., Parkos, C. A., and Nusrat, A. (2004). Role for actin filament turnover and a myosin II motor in cytoskeleton-driven disassembly of the epithelial apical junctional complex. Mol. Biol. Cell *15*, 2639–2651.

Jefferson, J. J., Leung, C. L., and Liem, R. K. (2004). Plakins: goliaths that link cell junctions and the cytoskeleton. Nat. Rev. Mol. Cell Biol. *5*, 542–553.

Kouklis, P. D., Hutton, E., and Fuchs, E. (1994). Making a connection: direct binding between keratin intermediate filaments and desmosomal proteins. J. Cell Biol. *127*, 1049–1060.

Kovacs, E. M., Goodwin, M., Ali, R. G., Paterson, A. D., and Yap, A. S. (2002). Cadherin-directed actin assembly: E-cadherin physically associates with the Arp2/3 complex to direct actin assembly in nascent adhesive contacts. Curr. Biol. *12*, 379–382.

Kovacs, M., Toth, J., Hetenyi, C., Malnasi-Csizmadia, A., and Sellers, J. R. (2004). Mechanism of blebbistatin inhibition of myosin II. J. Biol. Chem. *279*, 35557–35563.

Lewis, J. E., Wahl, J. K., 3rd, Sass, K. M., Jensen, P. J., Johnson, K. R., and Wheelock, M. J. (1997). Cross-talk between adherens junctions and desmosomes depends on plakoglobin. J. Cell Biol. *136*, 919–934.

Meng, J. J., Bornslaeger, E. A., Green, K. J., Steinert, P. M., and Ip, W. (1997). Two-hybrid analysis reveals fundamental differences in direct interactions between desmoplakin and cell type-specific intermediate filaments. J. Biol. Chem. *272*, 21495–21503.

Mertens, C., Hofmann, I., Wang, Z., Teichmann, M., Sepehri Chong, S., Schnolzer, M., and Franke, W. W. (2001). Nuclear particles containing RNA polymerase III complexes associated with the junctional plaque protein plakophilin 2. Proc. Natl. Acad. Sci. USA *98*, 7795–7800.

Noren, N. K., Liu, B. P., Burridge, K., and Kreft, B. (2000). p120 catenin regulates the actin cytoskeleton via Rho family GTPases. J. Cell Biol. *150*, 567–580.

O'Keefe, E. J., Briggaman, R. A., and Herman, B. (1987). Calcium-induced assembly of adherens junctions in keratinocytes. J. Cell Biol. *105*, 807–817.

Pasdar, M., and Li, Z. (1993). Disorganization of microfilaments and intermediate filaments interferes with the assembly and stability of desmosomes in MDCK epithelial cells. Cell Motil. Cytoskelet. *26*, 163–180.

Perez-Moreno, M., and Fuchs, E. (2006). Catenins: keeping cells from getting their signals crossed. Dev. Cell *11*, 601–612.

Pertz, O., Hodgson, L., Klemke, R. L., and Hahn, K. M. (2006). Spatiotemporal dynamics of RhoA activity in migrating cells. Nature *440*, 1069–1072.

Piekny, A., Werner, M., and Glotzer, M. (2005). Cytokinesis: welcome to the Rho zone. Trends Cell Biol. *15*, 651–658.

Pieperhoff, S., and Franke, W. W. (2008). The area composita of adhering junctions connecting heart muscle cells of vertebrates. VI. Different precursor structures in non-mammalian species. Eur. J. Cell Biol. *87*, 413–430.

Pokutta, S., Drees, F., Yamada, S., Nelson, W. J., and Weis, W. I. (2008). Biochemical and structural analysis of alpha-catenin in cell-cell contacts. Biochem. Soc. Trans. *36*, 141–147.

Ren, X. D., Kiosses, W. B., and Schwartz, M. A. (1999). Regulation of the small GTP-binding protein Rho by cell adhesion and the cytoskeleton. EMBO J. *18*, 578–585.

Reynolds, A. B., Daniel, J. M., Mo, Y. Y., Wu, J., and Zhang, Z. (1996). The novel catenin p120cas binds classical cadherins and induces an unusual morphological phenotype in NIH3T3 fibroblasts. Exp. Cell Res. *225*, 328–337.

Ridley, A. J., and Hall, A. (1992). The small GTP-binding protein rho regulates the assembly of focal adhesions and actin stress fibers in response to growth factors. Cell *70*, 389–399.

Sevilla, L. M., Nachat, R., Groot, K. R., and Watt, F. M. (2008). Kazrin regulates keratinocyte cytoskeletal networks, intercellular junctions and differentiation. J. Cell Sci. *121*, 3561–3569.

Shewan, A. M., Maddugoda, M., Kraemer, A., Stehbens, S. J., Verma, S., Kovacs, E. M., and Yap, A. S. (2005). Myosin 2 is a key Rho kinase target necessary for the local concentration of E-cadherin at cell-cell contacts. Mol. Biol. Cell *16*, 4531–4542.

Shimoyama, Y., Hirohashi, S., Hirano, S., Noguchi, M., Shimosato, Y., Takeichi, M., and Abe, O. (1989). Cadherin cell-adhesion molecules in human epithelial tissues and carcinomas. Cancer Res. *49*, 2128–2133.

Smith, E. A., and Fuchs, E. (1998). Defining the interactions between intermediate filaments and desmosomes. J. Cell Biol. *141*, 1229–1241.

Sobolik-Delmaire, T., Katafiasz, D., Keim, S. A., Mahoney, M. G., and Wahl, J. K., 3rd. (2007). Decreased plakophilin-1 expression promotes increased motility in head and neck squamous cell carcinoma cells. Cell Commun. Adhes. *14*, 99–109.

Sobolik-Delmaire, T., Katafiasz, D., and Wahl, J. K., 3rd. (2006). Carboxyl terminus of Plakophilin-1 recruits it to plasma membrane, whereas amino terminus recruits desmoplakin and promotes desmosome assembly. J. Biol. Chem. *281*, 16962–16970.

Stappenbeck, T. S., Bornslaeger, E. A., Corcoran, C. M., Luu, H. H., Virata, M. L., and Green, K. J. (1993). Functional analysis of desmoplakin domains: specification of the interaction with keratin versus vimentin intermediate filament networks. J. Cell Biol. *123*, 691–705.

Straight, A. F., Cheung, A., Limouze, J., Chen, I., Westwood, N. J., Sellers, J. R., and Mitchison, T. J. (2003). Dissecting temporal and spatial control of cytokinesis with a myosin II inhibitor. Science *299*, 1743–1747.

Symons, M. H., and Mitchison, T. J. (1991). Control of actin polymerization in live and permeabilized fibroblasts. J. Cell Biol. *114*, 503–513.

Takaishi, K., Sasaki, T., Kameyama, T., Tsukita, S., and Takai, Y. (1995). Translocation of activated Rho from the cytoplasm to membrane ruffling area, cell-cell adhesion sites and cleavage furrows. Oncogene *11*, 39–48.

Vaezi, A., Bauer, C., Vasioukhin, V., and Fuchs, E. (2002). Actin cable dynamics and Rho/Rock orchestrate a polarized cytoskeletal architecture in the early steps of assembling a stratified epithelium. Dev. Cell *3*, 367–381.

Vasioukhin, V., Bauer, C., Yin, M., and Fuchs, E. (2000). Directed actin polymerization is the driving force for epithelial cell-cell adhesion. Cell *100*, 209–219.

Vasioukhin, V., Bowers, E., Bauer, C., Degenstein, L., and Fuchs, E. (2001). Desmoplakin is essential in epidermal sheet formation. Nat. Cell Biol. *3*, 1076–1085.

Wahl, J. K., 3rd. (2005). A role for plakophilin-1 in the initiation of desmosome assembly. J. Cell Biochem. *96*, 390–403.

Wildenberg, G. A., Dohn, M. R., Carnahan, R. H., Davis, M. A., Lobdell, N. A., Settleman, J., and Reynolds, A. B. (2006). p120-catenin and p190RhoGAP regulate cell-cell adhesion by coordinating antagonism between Rac and Rho. Cell *127*, 1027–1039.

Yamada, S., and Nelson, W. J. (2007). Localized zones of Rho and Rac activities drive initiation and expansion of epithelial cell cell adhesion. J. Cell Biol. *178*, 517–527.

Yonemura, S., Hirao-Minakuchi, K., and Nishimura, Y. (2004). Rho localization in cells and tissues. Exp. Cell Res. *295*, 300–314.

Yonemura, S., Itoh, M., Nagafuchi, A., and Tsukita, S. (1995). Cell-to-cell adherens junction formation and actin filament organization: similarities and differences between non-polarized fibroblasts and polarized epithelial cells. J. Cell Sci. *108*, 127–142.

Zamansky, G. B., Nguyen, U., and Chou, I. N. (1991). An immunofluorescence study of the calcium-induced coordinated reorganization of microfilaments, keratin intermediate filaments, and microtubules in cultured human epidermal keratinocytes. J. Invest. Dermatol. *97*, 985–994.

Zhang, J., Betson, M., Erasmus, J., Zeikos, K., Bailly, M., Cramer, L. P., and Braga, V. M. (2005). Actin at cell-cell junctions is composed of two dynamic and functional populations. J. Cell Sci. *118*, 5549–5562.